Title:

Pneumococcus triggers NFkB degradation in COMMD2 aggresome-like bodies.

Authors: Michael G. Connor[1*], Lisa Sanchez[2], Christine Chevalier[1], Filipe Carvalho[3], Matthew G. Eldridge[1], Thibault Chaze[4], Mariette Matondo[4], Caroline M. Weight[5], Robert S. Heyderman[5], Jost Enninga[2], Melanie A. Hamon[1*].

Affiliations:

1 Chromatin and Infection, Institut Pasteur, Paris, France.
2 Dynamics of Host–Pathogen, Interactions Unit, Institut Pasteur, & UMR CNRS, Paris, France.
3 Institut MICALIS (UMR 1319) INRAE, AgroParisTech, Université Paris-Saclay
4 Institut Pasteur, Université de Paris Cité, CNRS UAR2024, Proteomics Platform, Mass Spectrometry for Biology Unit, 75015 Paris, France.
5 Division of Infection and Immunity, University College London, London, UK.

*Correspondence:
Michael G. Connor (mconnor@pasteur.fr) & Melanie A. Hamon (melanie.hamon@pasteur.fr)

Abstract:

NF-kB driven cellular immunity is essential for both pro- and anti-inflammatory responses to microbes, which makes it one of the most frequently targeted pathways by bacteria during pathogenesis. How NF-kB tunes the epithelial response to *Streptococcus pneumoniae* across the spectrum of commensal to pathogenic host phenotypic outcomes is not fully understood. In this study, we compare a commensal-like 6B ST90 strain to an invasive TIGR4 isolate and demonstrate that TIGR4 both blunts and antagonizes NF-kB activation. We identified, through comparative mass spectrometry of the p65 interactome, that the 6B ST90 isolate drives a non-canonical NF-kB RelB cascade, whereas TIGR4 induces p65 degradation though aggrephagy. Mechanistically, we show that during TIGR4 challenge a novel interaction of COMMD2 with p65 and p62 is established to mediate degradation of p65. With these results, we establish a role for COMMD2 in negative NF-kB regulation, and present a paradigm for diverging NF-kB responses to pneumococcus. Thus, our studies reveal for the first time a new bacterial pathogenesis mechanism to repress host inflammatory response though COMMD2 mediated turnover of p65.

Introduction:

The eukaryotic NF-kappaB family of transcriptional regulators are well documented for their potent ability to drive both pro- and anti-inflammatory cellular immune responses during microbe-host interaction [1-3]. As such, it is also one of the most frequently targeted host pathways during pathogenic infection. Of the three main documented NF-kB activation pathways - canonical, non-canonical and atypical- the canonical cascade is the most frequently documented as triggered and targeted for exploitation by bacteria [4-7].

The canonical pathway consists of NF-kB subunit heterodimers of p65/p50 or homodimers of p65/p65 bound to an inhibitory protein, such as IkBa. NF-kB subunits are normally sequestered in the cytoplasm in an inactive state [8]. Upon sensing of inflammatory molecules, such as cytokines (IL-1β or TNFα), pathogen-associated molecular patterns (PAMPs; i.e. lipopolysaccharide), and danger-associated molecular patterns (DAMPs; i.e. IL-1α or nuclear protein HMGB1) NF-kB subunits are rapidly activated by phosphorylation on serine residues (S536 and S276). Simultaneously, NF-kB dimers are released from their inhibitory IkB proteins and translocated to the nucleus of the cell for additional modification. Ultimately, this process leads to the binding of activated dimers to cognate NF-kB DNA motifs, thereby inducing NF-kB dependent gene transcription. NF-kB activation is tightly controlled for precise and rapid induction, but also for prompt repression. NF-kB dimers can be repressed through extraction, sequestration, and degradation from within the nucleus, while in parallel blocking cytoplasmic activation and promoting transcription of negative regulators [4,5,7,9-13]. However, in contrast to the myriad of studies on activators only a few negative regulators of NF-kB and their pathways have been documented.

COMMD (copper metabolism gene MURR1 domain)[14] proteins are among the select few negative regulators of NF-kB [12,14-19]. There are ten members of the COMMD family, all of which, interact with NF-kB to regulate signaling. The best-studied architype member, COMMD1, upon stimulation by TNF will lead to extraction of p65 from chromatin, followed by ubiquitination and proteasomal degradation. This process, functions independently of NF-kB nuclear translocation and IkBa, but through association with Cullin proteins, is able to terminate NF-kB signaling [12,14,16-22]. For the other COMMD proteins, however, neither their functional activity, their mechanism of NF-kB repression, or their interacting partners, outside of cullins, are known.

Unsurprisingly many bacterial species actively target the NF-kB pathway to repress the innate immune defenses of the host and support their survival. To date, all bacterial processes either coopt NF-kB repressors or directly target NF-kB pathway proteins using virulence factors (general review [3,23]). We and others have shown the obligate human pathobiont, *Streptococcus pneumoniae* (the pneumococcus), fine-tunes NF-kB signaling to support its interaction with the host, across the spectrum of commensal to pathogenic outcomes [24-30]. Surprisingly, we showed that a pathogenic *S. pneumoniae* strain showed very little NF-kB signaling compared to a colonizing, asymptomatic strain.

This observation raised the possibility that pneumococcus could subvert NF-kB signaling, which has not yet been documented.

Here, we demonstrate that a pathogenic TIGR4 pneumococcal strain [24], in contrast to a commensal-like 6B ST90 isolate [24], represses phosphorylation and activation of NF-kB p65. In fact, TIGR4 infection leads to specific degradation of p65 in airway epithelial cells, even upon stimulation with a strong inflammatory agonist, IL-1β. We performed an interactome of p65 and show that each pneumococcal strain interacts with diverging p65 interacting partners, revealing an original aggrephagy mechanism involving COMMD2 and p62. Therefore, we report a novel mechanism of pathogenesis to degrade p65 and repress the host response, specifically induced by TIGR4.

Results:

TIGR4 antagonizes NF-kB p65 activation.

Previously we showed a commensal-like 6B ST90 pneumococcal strain activated p65 to drive a unique inflammatory signature in comparison to a disease causing TIGR4 strain [24]. We showed that challenge with an invasive TIGR4 strain resulted in decreased transcriptional activation of several inflammatory cytokines [24,31], which suggested that NF-kB p65 activation was being disrupted by TIGR4. To directly measure NF-kB activation, we challenged A549 cells with either TIGR4 or 6B ST90 alone, or in combination with IL-1β, a pro-inflammatory stimulus known to drive p65 activation, by phosphorylation of the key serine residues 536 and 276 (review [10]). Cells were collected 2hr post-challenge for immunoblotting and the total levels of p65 were determined. Interestingly, upon infection with TIGR4, p65 levels significantly decreased compared to uninfected or 6B infected cells (Fig. 1A & B). It is important to note that p65 levels decreased even in the presence of IL-1β, which normally drives p65 activation.

Regardless of the total level of p65, we also evaluated the activity level of p65 by measuring phosphorylation at S536 and S276, under all conditions. TIGR4 was able to induce phosphorylation at S276, albeit at levels significantly lower than IL-1β alone, or 6B infection, but not at S536 (Fig. 1A, C, D). Importantly, time course monitoring of S536 phoshorylation, reveals that at no time point during infection, do the levels increase above uninfected levels (Sup. Fig. 1A). Taken together, these results show that TIGR4 is a poor activator of p65 in comparison to the 6B ST90 strain. Remarkably, the addition of IL-1β during TIGR4 infection did not restore phosphorylation of S536 or S276 to levels comparable to IL-1β alone, suggesting that infection with this strain of pneumococcus is actively antagonizing NF-kB signaling.

S. pneumoniae is an opportunistic respiratory pathogen. As such upper airway epithelial cells among the first to be encountered, which in turn triggers initial host responses. Therefore, we studied p65 levels and phosphorylation in primary human nasal epithelial cells (Sup. Fig. 1A) and nasopharyngeal Detroit 562 cells (Sup. Fig. 1B). Importantly, both of these cell types display the same blunting of NF-kB activation.

We further evaluated nuclear translocation of p65 by immunofluorescence, as this is a hallmark of p65 activation. Nuclear p65 intensity was quantified and normalized to the nuclear area by segmenting on the DAPI nuclear strain for TIGR4 (+/- IL-1β) against uninfected and IL-1β controls (Fig. 2A & B). In comparison to uninfected conditions, TIGR4 challenge caused slight nuclear recruitment of p65, but remained significantly lower ($pV \leq 0.001$) in comparison to IL-1β alone. Unexpectedly, there was a significant increase in nuclear p65 between TIGR4 + IL-1β and IL-1β alone (Fig. 2A & B), establishing that p65 is translocated in the TIGR4 + IL-1β condition even though phosphorylation levels are aberrant. It should be noted that this increase could be overestimated due to the cellular nucleus shrinking upon infection.

We then tested if aberrant activation and low translocation influenced downstream effector functions, namely transcription of p65 dependent genes. Total RNA was collected from A549 cells at 10, 30, 90, and 120 minutes post challenge with TIGR4 (+/- IL-1β) and IL-1β alone. Relative expression was determined for IL-6, IL-8, CFS2 and PTGS2 (COX-2) against uninfected/untreated controls at each time point. Surprisingly, TIGR4 infection alone did not lead to activation of any of the genes tested up

to 2h post challenge, in comparison to IL-1β alone (Fig. 2C). Furthermore, under conditions where IL-1β was added during TIGR4 challenge, there was both a delay and a repression of these transcripts in comparison to IL-1β alone. This was corroborated with the diminished p65 phosphorylation at S536 at the protein level at the same time points (Sup. Fig. 1A).

Transcriptional activation by p65 requires its binding to cognate kappa-biding sites at the chromatin level. Therefore, we evaluated levels of chromatin bound p65 at the locus of the NF-kB dependent gene *PTGS2*. Herein, chromatin was collected from A549 cells 2 hrs post-challenge with TIGR4 and the recovery of p65 quantified against uninfected and IL-1β controls by ChIP-qPCR targeting the two kappa-binding sites upstream of the *PTGS2* transcriptional start site (Fig. 2D). At both sites in TIGR4 challenged cells, there was less than 5% recovery of p65. This stands in contrast to the three-fold higher p65 recovery in IL-1β alone (Fig. 2E & F). Therefore, the lack of p65 driven transcription under TIGR4 challenge is intrinsically due to the absence of p65 at the chromatin.

Altogether, these data show the TIGR4 pneumococcal strain antagonizes p65 activation even in the presence of the pro-inflammatory cytokine, IL-1β. This creates a dysfunctional p65 signaling cascade leading to poor downstream activation of p65 dependent transcription.

A divergent NF-kB p65 interactome supports TIGR4 driven p65 degradation.

To begin to understand the NF-kB p65 activation differences between the two pneumococcal isolates we performed mass spectrometry of NF-kB p65 (Fig. 3A). Herein, an A549 GFP-p65 cell line was challenged with either TIGR4 or 6B ST90 and 2 hrs post-challenge GFP-p65 was immunoprecipitated with a matched A549 GFP alone control for mass spectrometry interactome analysis. From the analysis we identified p65 posttranslational modifications, as well as proteins interacting with p65 under the different conditions tested (Sup. Table 1).

The interactome data for 6B ST90 showed the sole NF-kB associated target was RelB, a major component of the non-canonical NF-kB pathway. Using whole cell lysates obtained from A549 cells 2 hrs post challenge with either 6B ST90 (+/- IL-1β) or TIGR4 (+/- IL-1β) we confirmed that RelB was significantly ($pV \leq 0.001$) elevated during challenge with 6B ST90 (+/- IL-1β) in comparison to both uninfected and TIGR4 (+/- IL-1β; Fig. 3B & C) and associated with p65 by co-immunoprecipitation (Sup. Fig. 2C).

In contrast, the TIGR4 challenged p65 mass spectrometry dataset enriched for different NF-kB associated targets. Gene Ontology and KEGG pathway analysis enriched for protein degradation pathways, including proteins such as HDAC6, a p62, and ubiquitin (Sup. Table 1) [32]. Indeed, p62 is a classical receptor of autophagy, HDAC6 an ubiquitin-binding histone deacetylase known to be important in modulating autophagy, and together have been shown to degrade protein aggregates through a process termed aggrephagy [32-34]. Therefore, our proteomic data suggested that p65 could be targeted for degradation through an aggrephagy pathway under TIRG4 infection conditions. To begin testing this hypothesis we probed whole cell lysates obtained from A549 cells 2 hrs post challenge with either 6B ST90 (+/- IL-1β) or TIGR4 (+/- IL-1β) for HDAC6 levels, as HDAC6 is degraded along with its cargo during aggrephagy (Fig. 3B & D). Indeed, only during TIGR4 challenge conditions did total HDAC6 levels decrease in comparison to uninfected, IL-1β alone and 6B ST90 groups. We then tested this hypothesis further using known chemical inhibitors to either proteasome or aggrephagy/lysosomal pathways. We treated cells with MG132 (10μM) [35], a general proteasome inhibitor, with Bafilomycin A1 (400nM) [36-38], an inhibitor of the terminal vATPase assembly during aggrephagy/lysosome fusion, or with SAR405 (500nM) [38,39], a PI3K inhibitor of the initiation of aggrephagy pathway, and assessed the levels of p65. Bafilomycin A1 and SAR405 treatments restored levels of p65 during TIGR4 challenge (+/- IL-1β) to comparable levels of uninfected and IL-1β alone (Fig. 3C), while MG132 had no effect in restoring p65 levels during TIGR4 challenge (Sup. Fig. 2A). The same trend for Bafilomycin A1 upon p65 levels 2 hrs post-challenge with TIGR4 was observed in primary human nasal epithelial cells (Sup. Fig. 2B). These data, along with the identification of HDAC6 and p62 in the p65 interactome strongly suggest that TIGR4 is inducing degradation of p65 through an aggrephagy pathway.

We further determined if degradation was restricted to only the p65 subunit or was also impacting the levels p50, which in a heterodimer with p65 is the primary translocated unit to the nucleus [5]. We immunoprecipitated endogenous p65 from A549 cells challenged with 6B ST90 or TIGR4 against uninfected and IL-1β and probed for the p50 subunit. Already in the input, the levels of p50 is lower upon infection with TIGR4 compared to 6B ST90, which is also noticeable from the immunoprecipitation (Sup. Fig. 2C). This observation further supports that TIGR4 challenge is targeting NF-kB p65 complex as a whole.

Overall, these data demonstrate TIGR4, in contrast to 6B ST90, induces diverging NF-kB p65 signaling cascade that results in: 1) differential protein binding, 2) degradation of p65 through aggrephagy.

COMMD2 associates with both p65 and p62 and translocates to the nucleus

The COMMD1 protein has previously been shown to terminate NF-kB signaling through proteasomal degradation [16,17,19,21,40]. Our interactome identified COMMD2 and COMMD4 as among the most highly enriched proteins associating to p65 under TIGR4 infection conditions compared to 6B ST90. COMMD2 and COMMD4 were previously shown to associate with p65 and NFkB1 [14], and other members of this protein family have a repressive role in NFkB signaling [12,16-18,20,22]. Therefore, we hypothesized that COMMD2 and COMMD4, through their association with p65, could be involved in p65 turnover through a similar aggrephagy pathway.

With no robust COMMD2 antibody commercially available for co-immunoprecipitation or immunoblot, we generated an A549 GFP-COMMD2 ectopic expression stable cell line, from which GFP-COMMD2 was immunoprecipitated from lysates 2 hrs post-challenge with either 6B ST90 (+/- IL-1β), TIGR4 (+/- IL-1β) or from our uninfected and IL-1β controls. Samples were probed for p65 or p62 to detect interaction with COMMD2. Our results show that only under TIGR4 challenge conditions do p65 and p62 interact with COMMD2 (Fig. 4A & B). Furthermore, upon addition of IL1β, p65 interacts with COMMD2 to even higher levels. Therefore, COMMD2 is a new infection specific interacting partner of p65, making a complex of p65-COMMD2-p62.

Although infection with TIGR4 leads to p65 degradation, the small amount left in the cell is nuclear (Fig. 1E). Therefore, to evaluate the cellular localization of the p65-COMMD2-p62 we performed immunofluorescence experiments using the GFP-COMMD2 A549 cell line. Using this cell line, we further determined infection induced effect on p62. The GFP-COMMD2 A549 cell line was challenged with TIGR4 (+/- IL-1β) and compared to uninfected and IL-1β controls, followed by paraformaldehyde fixation and probing for p62. Total p62 levels in the nucleus were determined per cell, by segmentation on the GFP-COMMD2 signal for the cellular cell boundaries and DAPI for the nucleus (Fig. 4C). There was a significant ($pV \leq 0.001$) decrease in total p62 levels for TIGR4 challenged cells (+/- IL-1β) in comparison to both uninfected and IL-1β alone (Fig. 4D), which is expected upon activation of protein degradation pathways. Interestingly, there is a reciprocal increase in the nuclear levels of p62 (Fig. 4E), showing that during TIGR4 challenge there is movement of p62 between the cytoplasm and nuclear compartments in addition to degradation. Moreover, we noticed COMMD2, an otherwise cytoplasmic protein was translocated in the nucleus of cells challenged with TIGR4 (+/- IL-1β) (Fig. 4C). Similarly to p62, there was a decrease in total COMMD2 levels, indicative of protein turnover, and an increase of COMMD2 in the nucleus (Fig. 4F & G).

We confirmed our microscopy observation by performing cell fractionations. We immunoblotted cell fractions obtained from the GFP-COMMD2 stable cell line 2 hrs post-challenge with TIGR4 (+/- IL-1β) as well as from uninfected and IL-1β controls (Fig. 4H & I). Whereas cells treated with IL-1β alone displayed 20% COMMD2 in the nucleus, similar to untreated/uninfected cells, TIGR4 (+/- IL-1β) challenge conditions had 80% of COMMD2 consistently nuclear (Fig. 4I). The levels of cytoplasmic COMMD2 under TIGR4 (+/- IL-1β) challenge conditions correspondingly decreased, demonstrating a relocalization of COMMD2. Finally, we tested if the commensal-like strain 6B ST90 could also induce COMMD2. Using cellular fractionation and immunoblotting, we show that 6B ST90 was incapable of triggering nuclear localization of COMMD2 (Sup. Fig.3A), which demonstrates

relocalization is TIGR4 specific. Strikingly, upon challenge with TIGR4, we observed perinuclear COMMD2 puncta formation. Such puncta of protein aggregates, along with a decrease in p62 levels have previously been described [41-45] and further support our findings that TIGR4 is activating aggrephagy during infection.

To further test if inhibiting terminal stages of aggrephagy would restore p62 levels, we treated cells with Bafilomycin A1 (400nM) and collected whole cell lysates 2 hrs post-challenge with either IL-1β alone or TIGR4 (MOI 20). Samples were immunoblotted for p62 and actin for quantification. The results showed Bafilomycin A1 treatment blocked p62 degradation during TIGR4 challenge restoring it to comparable uninfected levels (Sup. Fig. 3A), further demonstrating that TIGR4 challenge triggers p65 turnover through an infection induced p65-COMMD2-p62 complex.

TIGR4 mediated COMMD2 nuclear translocation is dependent on Ply.

Our data show a strain specific degradation of p65 and relocalization of COMMD2, suggesting intrinsic factors to TIGR4 challenge were responsible for these effects. Thus, we tested TIGR4 mutants of Pneumolysin (Ply) and Pyruvate oxidase (SpxB), two major pneumococcal virulence factors we have previously shown to affect host cell signaling at the nuclear level [46-48]. A549 GFP-COMMD2 stable cell line was challenged for 2 hrs with either wildtype TIGR4, TIGR4Δply or TIGR4ΔspxB and the nuclear levels of COMMD2 quantified against uninfected and IL-1β alone. Nuclear COMMD2 levels were measured by deconvoluted epifluorescence, and quantified by measuring signal intensity normalized by nuclear area by segmenting the nucleus using DAPI stain (Fig. 5A & B). These data show COMMD2 was found primarily within the cytoplasm of uninfected and IL-β treated cells, and translocated to the nucleus upon TIGR4 challenge. Similar levels of nuclear translocation were obtained with the *ΔspxB* mutant, indicating that pneumococcal pyruvate oxidase and peroxide production is not necessary for COMMD2 localization. However, deletion of the PLY toxin completely abrogated nuclear translocation, indicating that this bacterial factor is essential (Fig. 5B). Since the 6B ST90 strain does not lead to nuclear translocation of COMMD2 (Sup. Fig.3A), we concluded that although Pneumolysin is essential, it is not sufficient, since 6B ST90 produces the same amount of this toxin as TIGR4 [24].

COMMD2 exports p65 for lysosomal degradation.

COMMD2 has two nuclear export signal domains and no predicted nuclear localization signal domains, suggesting a function for this protein in the cytoplasm, where aggrephagy degradation has been shown to occur [33,34,49]. Thus, we postulated COMMD2 was involved with nuclear export of aberrantly phosphorylated p65 under TIGR4 challenge. This mechanism of action would be similar to the architype family member COMMD1, which binds NF-kB in the nucleus and exports it through CRM1 for degradation [12,22]. Therefore, we tested whether COMMD2 was exported through CRM1 by using the Leptomycin B inhibitor [50]. GFP-COMMD2 cells were treated with Leptomycin B (10 nM), and immunofluorescence was used to image p62 and p65. Strikingly, by blocking nuclear export we observed that COMMD2 was now localized to the nucleus in uninfected and IL-1β treated cells. Similarly, p62 and p65 are relocalized to the nucleus. In fact, COMMD2 and p62 were detected in puncta in the nucleus (Fig. 6A), where p65 was localized (Fig. 6B). Notably, our IL-1β positive pro-inflammatory stimulus control, known to drive nuclear translocation of p65, had a significant ($pV \leq 0.0001$) increase in the nuclear level of COMMD2 and p62 in comparison to uninfected cells (Fig. 6C & D). These surprising data suggest that under nuclear export stress, COMMD2 and p62 are naturally recruited to the nucleus at specific puncta through a defined process.

Interestingly, upon challenge with TIGR4, Leptomycin B treated cells displayed higher levels of COMMD2 and p62 accumulation in the nucleus than without treatment (Fig. 6A, C & D). Thus, upon inhibiting nuclear export of COMMD2 and p62, these proteins are no longer being degraded upon infection and accumulate in the nucleus. Similarly, Leptomycin B inhibition also increased the nuclear p65 levels in all conditions compared to untreated cells (Fig. 6E), and even restored p65 levels to those of cells stimulated with IL-1β alone. Although COMMD2 puncta are observed upon addition of Leptomycin B, the substantial amount of p65 trapped within the nucleus of these cells rendered

definitive scoring of puncta and colocalization difficult and was not done. Furthermore, under conditions of TIGR4+ IL-1β and Leptomycin B inhibition, we observed a significant (pV ≤ 0.0001) increase in p62 puncta compared to TIGR4 alone (Fig. 7A & B). These data therefore show that without Leptomycin B inhibition TIGR4 challenge leads to an active CRM1 dependent export of p65. Altogether, these results imply that p65 is exported from the nucleus via COMMD2 – p62 dependent process upon challenge with TIGR4.

Nuclear export must precede protein turnover, which occurs in the cytoplasm. To confirm that COMMD2 and p62 were degraded through the same lysosomal turnover we described in figure 3E, we treated GFP-COMMD2 cells with Bafilomycin A1 (400nM; pre-treated for 3 hrs) and quantified the total levels of p65, p62 and COMMD2 per cell 2 hrs post-challenge with either IL-1β or TIGR4 (+/- IL-1β; MOI 20) using confocal microscopy. Similarly to figure 3E, TIGR4 challenged cells (+/- IL-1β) treated with Bafilomycin A1 displayed an increase in p65, but also COMMD2, and restored p62 levels comparably to uninfected controls (Fig. 7C - E). Moreover, in contrast to uninfected and IL-1β treated cells there was a significant (pV ≤ 0.0001) increase in both p65 and COMMD2 levels in TIGR4 conditions. Therefore, the COMMD2-p65-p62 complex is being degraded through aggrephagy-mediated turnover upon TIGR4 challenge and is amplified in the presence of the pro-inflammatory stimulus IL-1β.

Discussion:

Cellular inflammatory response is a critical component of the host defense to bacteria. Yet, the molecular processes that fine-tune NF-kB cascades across the range of colonizing to virulent bacteria is poorly understood. Herein, we show that an invasive *S. pneumoniae* TIGR4 strain, which causes symptomatic disease in murine models [24], blunts p65 activation and inflammatory gene transcription in comparison to a commensal-like asymptomatic 6B ST90 strain, that activated p65 [24]. Through mass spectrometry, interactome and post-translational modification analysis, we show these two pneumococcal isolates have diverging p65 interacting partners and phosphorylation status. We show the 6B ST90 strain upregulates RelB, a hallmark of non-canonical NF-kB signaling, whereas the p65 interactome for the invasive TIGR4 strain enriched for aggrephagy pathway components. Mechanistically, we reveal that p65 is being degraded through a unique TIGR4 induced interaction of COMMD2 with p65 and p62. Altogether, this is the first demonstration of a bacterial pathogenesis mechanism to repress inflammatory gene transcription through targeted degradation of NF-kB p65.

Negative regulation of NF-kB signaling, in contrast to the breadth of knowledge on activatory mechanisms, is poorly documented. This is in part due to the lack of identified targets and mechanisms responsible for attenuating this signaling cascade. Of the known negative regulators, A20 (TNAIP3) and COMMD1 are the better described. A20 is primarily a deubiquitinase whose transcription is NF-kB activation dependent. A20 functions in a negative feedback loop to deubiquintinate NEMO, which results in its stabilization with the IKK complex to restore NF-kB sequestration in the cytoplasm. This ultimately terminates the downstream canonical NF-kB signaling cascade of inflammatory response [5,12,51]. In contrast, COMMD1 transcription is NF-kB independent, and facilitates p65 termination by CRM1 mediated export and translocation of p65 to the proteasome for degradation via complex formation of COMMD1 with Elongins B & C, Cullin2 and SOCS1 (ECS^{SOCS1}) [14,16,17,19,21,22]. In parallel, COMMD1 contributes to repression of p65 driven gene transcription by occupying the formerly p65 bound kappa-binding site at specific gene promoters [20]. It was put forth that the diversity of potential COMMD, NF-kB and cullin assemblies and the array of physiological stimuli activating such complex formations positioned this family of proteins as potent selective negative regulators of NF-kB signaling. Our work is the first to show a role for COMMD2 in p65 turnover through p62 and aggrephagy. This new negative feedback mechanism on p65 may represent, even in a cellular state without bacterial infection, a precise mechanism to terminate or shift a given p65 dependent transcription repertoire. Additionally, by lowering the amount of p65 protein present through degradation, a lower threshold of inhibitory IKK proteins would be needed to quench this cascade within the cell. This could rapidly shift the balance in favor of IKK proteins sequestering p65, and perhaps even favor a switch in NF-kB

heterodimers, leading to activation of a different transcriptional repertoire. In essence, such inhibition would be quite potent, as inflammatory transcription, inflammatory signal sensing, and negative inflammatory feedback are all blocked simultaneously. Such a mechanism would greatly favor pathogenic infection and host cell exploitation, as we observe upon TIGR4 challenge.

To date the molecular mechanism induced by TIGR4 challenge is the only stimulus to trigger COMMD2-p62-p65 complex formation. On the other end of the virulence spectrum, the commensal like 6B ST90 strain lead to the formation of a p65-RelB complex. Therefore, such interactome studies, in combination with pro-inflammatory stimulus, will reveal new partners that govern p65 regulation. In addition, the vast array of post-translational modifications on p65 and other NF-kB subunits across differential stimulations has given rise to the "NF-κB barcode hypothesis", which suggests that distinct patterns are linked to how inflammatory gene transcription occurs [52,53]. We show here that bacterial stimuli are ideal tools to dissect the complexity of this signaling cascade and opens up the field of research in NF-kB signal termination.

Supporting this is our exploratory mass spectrometry of p65 phosphorylation, which identified serine 45 (S45) as the only enriched phosphorylated mark during TIGR4 challenge. This mark has previously been shown to negatively regulate p65, although the mechanism is unknown [54]. Lanucara et al., showed that a phosphomimetic mutant of S45 prevented IL-6 transcription and p65 binding to the promoter under TNFα stimulation [54]. It remains to be evaluated if this modification is involved in COMMD2-p62 degradation of p65 and therefore could alter the host response to pneumococcus. Interestingly, the commensal-like 6B ST90 does not induce phosphorylation of this residue. Instead, this strain leads to phosphorylation on S203 and activation of the chromatin modifier KDM6B to drive containment in the upper respiratory tract [24]. Whether differential phosphorylation of p65 is the determining factor in the ultimate host response to different strains of pneumococcus remains to be determined. In this context it is tempting to speculate that posttranslational modifications of p65 could represent markers of either host response to commensal or to invasive bacteria.

Tuning NF-kB dependent immune gene transcription is fundamental for cellular immune processes of airway epithelial cells exposed to pneumococcus [25,55]. The pro-inflammatory cytokines, TNFα and IL-1β, are major cytokines necessary for neutrophil recruitment and are found in bronchoalveolar lavage fluid of animals challenged with pneumococcal isolates [25,55,56]. However, one study showed that when isolated, murine lung epithelial cells exposed to serotypes 19 and 3 failed to induce p65 (RelA) nuclear translocation in comparison to TNFα and IL-1β [25]. Our studies directly address this paradox showing that the invasive TIGR4 pneumococcal isolate is actively engaged in repressing p65 signaling through degradation even in an environment containing pro-inflammatory stimuli. We propose that pneumococcus interaction with the 'primary' contacted host epithelial cell results in repressed NF-kB signaling with simultaneous prevention of negative feedback upon this inflammatory response. However, what has been shown during respiratory infection with other microbes [57,58], is that a balance is needed between pro-inflammatory responses and negative regulation to ensure minimal tissue damage from the influx of neutrophils into the airway tissues [56]. Airway epithelial cells play a crucial role in both situations by regulating neutrophil recruitment and promoting epithelial repair pathways leading to tissue resilience and resolution of inflammation [55,56,59,60]. With pneumococcus actively antagonizing the ability of airway epithelial cells to both induce and respond to IL-1β we hypothesize an amplifying and runaway inflammatory cascade is created in latter stages of infection where neutrophil influx is detrimental [55,60,61]. This could lead to exacerbated and severe pneumonia with excessive tissue damage allowing pneumococcus to transmigrate through the lungs and into deeper tissues. We put forth that COMMD2, or combinations of COMMD proteins are potent modulators of bacterial driven inflammatory processes, and may represent a novel therapeutic target to avoid runaway inflammation.

In conclusion, our study shows a new regulatory role for COMMD2 in restraining p65 through aggrephagy mediated turnover triggered by bacterial interaction. We reveal this process to be specific to invasive pneumococcal challenge and partially depend on pneumolysin. Further studies charactering both the p65 and COMMD2 interactome under bacterial challenge with isolates

representing divergent pneumococcal host interaction may identify new processes exploited at the microbe-host interface to regulate NF-kB signaling and identify novel negative regulators of inflammation.

Materials and methods:

Bacteria strains, growth, and enumeration. Serotype 6B ST90 CC156 lineage F (ST90; CNRP# 43494) and TIGR4 were obtained from the Centre National de Référence des Pneumocoques (Emmanuelle Varon; Paris, France) and (Thomas Kohler, Universität Greifswald) respectively. Experimental starters were made from master glycerol stocks struck on 5% Columbia blood agar plates (Biomerieux Ref# 43041) and grown overnight at 37°C with 5% CO_2 prior to outgrowth in Todd-Hewitt (BD) broth supplemented with 50 mM HEPES (Sigma) (TH+H) as previously described [24]. Inocula were prepared from frozen experimental stocks grown for 3 – 4 hrs to midlog phase in TH+H at 37°C with 5% CO_2 in closed falcon tubes. Bacterial cultures were pelleted at 1,500xg for 10 mins at room temperature (RT), washed in DPBS, and concentrated in 1mL DPBS prior to dilution at desired CFU/mL using 0.6 OD_{600} /mL conversion factors in desired cell culture media [24]. Bacterial counts were determined by serial dilution plating on 5% Columbia blood agar plates and grown overnight at 37°C with 5% CO_2.

Cell culture conditions and in vitro challenge. A549 human epithelial cells (ATCC ref# CCL-185) and A549 stable cell lines were maintained in F12K media (Gibco) supplemented with 1x GlutaMax (Gibco) and 10% heat inactivated fetal calf serum (FCS) at 37°C with 5% CO_2. Detroit 562 human nasopharyngeal epithelial cells (ATCC ref# CCL-138) were maintained in DMEM supplemented with 1x sodium pyruvate (Gibco) and 1x GlutaMax (Gibco) 10% heat inactivated FCS. Primary human nasal epithelial cells (HNEpC; PromoCell ref# C-12620) were cultured and maintained in Airway Epithelial Cell Growth Medium (PromoCell ref# C-21060). All cell lines were discarded after passage 15, and HNEpC discarded after passage 4. For challenge studies cells were plated in tissue culture treated plates at $2x10^5$ cells (6well; for 72 hrs), $5x10^4$ cells (24well; for 48 hrs), or $1x10^4$ cells (96well; for 48 hrs) [24]. Bacterial inocula (Multiplicity of infection (MOI) 20) were diluted in cell culture media, added to cells, and bacterial-epithelial cell contact synchronized by centrifugation at 200xg for 10 mins at RT. Plates were moved to 37°C with 5% CO_2 for 2 hrs and processed as desired for experiment termination. For inhibitor studies, cell culture media was aspirated, and replaced with filter sterilized culture media containing either of the inhibitors MG132 10 µM final concentration (Sigma ref# M7449), Bafilomycin A1 400 nM final concentration (Sigma ref# SML1661) or Leptomycin B 10 nM final concentration (Sigma ref# L2913) for 3 hrs prior to bacterial addition. Human IL-1β (Enzo Life Sciences ref# ALX-522-056) was used at 10 ng/mL final concentration in cell culture media.

RNA isolation and RT-qPCR. Total RNA isolated and extracted using TRIzol (Life technologies ref#15596-026) method as per manufacturer's recommendations. Recovered RNA (5 µg) was converted to cDNA with Super Script IV as per manufacturer's instructions, diluted to 20 ng/µL in molecular grade water and 1 µL used for Sybr Green reactions as per manufacturer's instructions on a BioRad CFX384 (BioRad). Relative expression was calculated by ΔΔCt method to *GapDH* [62]. RT-PCR primers listed in Sup. Table 2.

ChIP and ChIP-qPCR. Detailed ChIP buffer components and procedure were completed as previously reported [24]. Briefly, $8x10^6$ A549 cells were cross-linked with 1% formaldehyde at room temperature and quenched with 130 mM glycine. Chromatin was generated from the collected cell pellets by lysis and sonication in chromatin shearing buffer to a size of 200-900bp. ChIP grade antibody to p65 (L8F6) (CST ref #6956) was used at manufacturer's recommended concentrations and bound to DiaMag beads (diagenode ref # C03010021-150) overnight with gentle rotation. Quantified chromatin was diluted to 10 µg per immunoprecipitation and added to antibody bound DiaMag beads overnight with gentle rotation and 8% of input reserved. Beads were washed as previously described [24], and DNA purified using phenol-chloroform extraction followed by isopropanol precipitation. Recovered DNA

suspended in molecular grade water was used for Sybr Green reactions (1 µL) on a BioRad CFX384 (BioRad). ChIP-qPCR primers (50-150 bp; 60 °C max melt temperature) were designed to span the NF-κB sites of interest within the promoters of *PTGS2* [63]. % recovery was calculated as 2 raised to the adjusted input Ct minus IP Ct multiplied by 100. ChIP qPCR primers listed in Sup. Table 2.

Plasmids, molecular cloning and stable cell line generation. All plasmids and primers are listed in Sup. Table 2. Routine cloning was carried out by in vivo assembly [64,65]. Briefly, primers were designed with a 15-20 bp overlap to amplify nucleic acid targets using Phusion Plus polymerase (Thermo ref# F630S). Correct sized bands were excised and nucleic acid extracted by "Freeze and squeeze" [66,67]. Herein, 0.7% - 1% agarose gel fragments were frozen for 5 mins on dry ice and centrifuged for 15 mins at >21,000 xg with the supernatant collected – the process was completed two additional times. Collected supernatant containing nucleic acid was then purified using phenol-chloroform extraction followed by isopropanol precipitation and suspension in molecular grade water. Collected nucleic acid was quantified spectrophotometrically using a NanoDrop and mixed at 3:2 (vector : insert) in 10 µl and added to chemically competent E. coli MC1061 or DH5α for transformation. After 1 hr incubation on ice bacteria outgrowth was done for 1 hr in Luria-Bertani (BD) prior to selection on LB agar containing desired antibiotic (Sup. Table 2). All plasmids were isolated with the QIAprep Spin Miniprep Kit (Qiagen ref# 27106) and eluted in molecular grade water (endotoxin free) as per manufacturer's instructions. A549 stable cell lines were generated using the transposon-based sleeping beauty system [68,69]. A549 cells were plated in tissue culture treated plates at $2x10^5$ cells (6well) one day prior to transfection with 2 µg plasmid DNA + 150 ng SB100 transposase DNA. After transfection, cells were selected with 1 mg/mL Geneticin (Thermo ref# 10131035) for 7 days, with media exchanged on days 1, 3, 5 & 7. Selected cells were collected with Trypsin 0.25% EDTA (Thermo ref# 25200056) and two-way serial diluted in a 96 well tissue culture plate for monoclonal selection for another 7 – 14 days with media containing 1 mg/mL Geneticin and exchanged every 2 – 3 days. Selected colonies were expanded and FACS sorted to ensure purity, uniform expression, and comparison of intensity for selecting a robust clone for subsequent experiments.

Immunoblots and quantification. Whole cell lysates were obtained by RIPA lysis (10 mM Tris HCL pH 7.5, 150 mM EDTA, 0.1% SDS, 1% Triton X-100 & 1% Deoxycholate) supplemented with inhibitor cocktail (1X PhosSTOP, 10 mM sodium butyrate, 0.2 mM PMSF). Samples combined with 5x with Laemmli buffer [70], sonicated for 5 mins in a ultrasonic water bath, boiled at 98°C (dry bath) for 10 mins and frozen at -20°C. Whole cell lysates were ran on 4 – 20% pre-cast polyacrylamide SDS PAGE gels (BioRad), transferred to PVDF membrane (BioRad TransBlot) and blocked 1 hr in 5% BSA TBST at room temperature. Membranes were probed overnight at 4°C in 5% BSA TBST with primary antibody to p65 (CST ref #6956 or CST ref# 8242), p65 phosphorylation at serine 536 (CST ref# 3033), p65 phosphorylation at serine 276 (abcam ref# ab183559), NFkB p105 / p50 (abcam ref# ab32360), RelB (abcam ref# ab180127) or actin AC-15 monoclonal (Sigma ref# A5441) as per manufacturer's recommendations. Incubated for 1 hr at room temperature with appropriate secondary-HRP conjugated antibodies in 5% Milk TBST and developed with clarity ECL (BioRad) developing reagents with a ChemiDoc Touch (BioRad). Detroit562 immunoblots were developed using Licor Odessey using secondary antibodies at 1:7,500 - Goat anti-rabbit IgG H&L (IRDye 800CW) and goat anti-mouse IgG H&L (IRDye 680RD) from abcam. Band intensity was quantified by Image Lab (BioRad), or using Fiji [71] (Detroit 562 cells) with linear intensity values $\log_{10}$ transformed and normalized to actin prior to any additional ratio metric comparisons.

Cell fractionation. Fractionation was performed as previously described as previously described [24]. Faction lysates were combined with 5x with Laemmli buffer [70], sonicated for 5 mins in a ultrasonic water bath, boiled at 98°C (dry bath) for 10 mins and frozen at -20°C. Samples were ran on either 10% (for GFP-COMMD2) or 12% (for fraction quality controls) polyacrylamide SDS PAGE gels (BioRad), transferred to PVDF membrane (BioRad TransBlot), blocked 1 hr in 5% BSA TBST at room temperature.

Primary antibody in 5% BSA TBST to GFP (abcam ref# ab290), GapDH (abcam ref# ab8245), or histone H4 (abcam ref# ab177840) was completed overnight at 4°C. After 3x 10 min washes in TBST appropriate secondary-HRP conjugated antibodies in 5% Milk TBST were incubated for 1 hr at room temperature and developed with a ChemiDoc Touch (BioRad) as described above.

Immunofluorescence microscopy and Cellprofiler analysis. For microscopy the desired cell line were seeded on acid washed and UV treated coverslips in 24well or 96well plates as described above. Two hours post-challenge media was aspirated, cells washed in DPBS, and fixed with 2.5% PFA for 10 mins at RT. Fixed cells were blocked and permeabilized overnight in 5% BSA 0.5% Tween20 at 4°C. Primary antibody to p65 (CST ref #6956 or CST ref# 8242), COMMD2 (Sigma ref# HPA044190-25UL; only works for immunofluorescence), or p62 (SQSTM1; abcam ref# ab109012) were diluted at 1:1,000 in 5% BSA 0.5% Tween20 and incubated overnight at 4°C. Cells were washed 3x 10 mins at RT in PBS + 0.1% Tween20 prior to 1 hr incubation at 1:1,000 dilution of either Alexa Fluor 594 or Alexa Fluor 647 secondary antibody. Nuclei were stained with 10 ng/mL final concentration of Hoechst 33342 for 15 mins. Coverslips were rinsed in PBS and molecular grade water prior to mounting with Fluoromount-G Mounting Medium (INTERCHIM). Confocal microscopy images were acquired on a Nikon TiE inverted microscope with an integrated Perfect Focus System (TI-ND6-PFS Perfect Focus Unit) and a Yokogawa Confocal Spinning disk Unit (CSU-W1). Nine images per well were acquired using a 20X air objective (NA 0.75) at a step-size of 0.9µm in z-plane. Deconvoluted epifluorescent images were acquired on a Cytation 5 (BioTek) using a 20X air objective (NA 0.75) with a grid of 3 x 3 (9 images en total).

Images were processed for background using Fiji [71], and segmented using Cell Profiler [72-74]. Briefly, the pipeline for image analysis consisted of sequential modules to 'IdentifyPrimaryObjects' based on channel signal for nuclei (DAPI stain), p65 (Alexa594), or p62 (Alexa594). This was followed by 'IdentifySecondaryObjects' for the GFP-COMMD2 signal via propagation of identified nuclei. Objects were related to each other to maintain cohesion between identified nuclei, cell and cellular contents (p65 or p62). For puncta, the additional module, 'EnhanceorSupressFeatures' with 'Speckles', was used. This used a global threshold strategy with Otsu threshold method and a 2% minimum boundary to identify puncta contained within the segmented nuclei.

Immunoprecipitation. Cells were lysed in 250 µL of RIPA lysis (10 mM Tris HCL pH 7.5, 150 mM EDTA, 0.1% SDS, 1% Triton X-100 & 1% Deoxycholate) supplemented with a protease mixture inhibitor (Roche Complete, EDTA free). Lysates were either immunoprecipitated using GFP-trap agarose beads (ChromoTek ref# gta-10) or with slurry protein G beads (Sigma-Aldrich Fast Flow Protein G sepharose). For GFP-p65 and GFP-COMMD2 the samples were immunoprecipitated as per manufacturer's instructions with the elution was recovered in either 5x with Laemmli buffer [70] and boiled at 98°C (dry bath) for 10 mins, or left in Trypsin digest buffer (see LC-MS/MS Mass-spectrometry and analysis). All samples were frozen at -20°C. For endogenous samples the lysates were incubated on a rotating wheel at 4 °C for 20 min before adding 1 mL of dilution buffer (150 mM NaCl and 50 mM Tris-HCl pH 7.5 supplemented with Protease mixture inhibitor) to reduce the detergent final concentration below 0.1%. The lysates were then centrifuged at 10,000 × g for 10 min, and the insoluble pellet was discarded. For p65 IP the lysates were then incubated with 2 µg of antibody CST ref #6956 or CST ref# 8242) at 4 °C for 2 hrs before adding 20 µL of slurry protein G beads (Sigma-Aldrich Fast Flow Protein G sepharose) for 20 min. The beads were then washed before adding 20 µL of Laemmli buffer supplemented with 2% β-mercaptoethanol and boiled for 5 min.

LC-MS/MS Mass-spectrometry and analysis. For label-free quantitative proteomic analysis of GFP-p65 and GFP-COMMD2 the respected A549 cell lines were plated in 6well tissue culture plates, and challenged with bacteria for 2hrs as described above. One plate (~$5x10^7$ cells) per condition was harvested using RIPA lysis and immunoperciptated with GFP-trap agarose beads (ChromoTek ref# gta-10) as per manufacturer's instructions. Three or four independent biological replicates were prepared

and analyzed for each condition. Prior to on-bead Trypsin digestion, the samples were washed 3x in trypsin digest buffer (20 mM Tris.HCl pH 8.0, 2 mM $CaCl_2$). On bead digestion was performed strictly as described by Chromotek. Briefly, beads were suspended in digestion buffer (Tris 50 mM pH 7.5, urea 2 M, 1 mM DTT and 5 µg.µl of trypsin (Promega)) for 3 min at 30°C. Supernatants were transfer to new vials and beads were washed twice using (Tris 50 mM pH 7.5, urea 2 M and iodoacetamide 5 mM). All washes were pulled and incubated at 32°C for overnight digestion in the dark. Peptides were purified using C18 stage tips protocol [75].

LC-MS/SM analysis of digested peptides was performed on an Orbitrap Q Exactive Plus mass spectrometer (Thermo Fisher Scientific, Bremen) coupled to an EASY-nLC 1200 (Thermo Fisher Scientific). A home-made column was used for peptide separation (C_{18} 30 cm capillary column picotip silica emitter tip (75 µm diameter filled with 1.9 µm Reprosil-Pur Basic C_{18}-HD resin, (Dr. Maisch GmbH, Ammerbuch-Entringen, Germany)). It was equilibrated and peptide were loaded in solvent A (0.1 % FA) at 900 bars. Peptides were separated at 250 $nl.min^{-1}$. Peptides were eluted using a gradient of solvent B (80% ACN, 0.1 % FA) from 3% to 31% in 45 min, 31% to 60% in 17 min, 60% to 90% in 5 min (total length of the chromatographic run was 82 min including high ACN level step and column regeneration). Mass spectra were acquired in data-dependent acquisition mode with the XCalibur 2.2 software (Thermo Fisher Scientific, Bremen) with automatic switching between MS and MS/MS scans using a top 12 method. MS spectra were acquired at a resolution of 70000 (at *m/z* 400) with a target value of 3×10^6 ions. The scan range was limited from 300 to 1700 *m/z*. Peptide fragmentation was performed using higher-energy collision dissociation (HCD) with the energy set at 27 NCE. Intensity threshold for ions selection was set at 1×10^6 ions with charge exclusion of z = 1 and z > 7. The MS/MS spectra were acquired at a resolution of 17500 (at *m/z* 400). Isolation window was set at 1.6 Th. Dynamic exclusion was employed within 30 s.

Data were searched using MaxQuant (version 1.5.3.8) using the Andromeda search engine[76] against a human database (74368 entries, downloaded from Uniprot the 27th of September 2019), a Streptococcus pneumoniae R6 database (2031 entries, downloaded from Uniprot the 1st of January 2020) and a Streptococcus pneumoniae serotype 4 database (2115 entries, downloaded from Uniprot 1st of January 2020).

The following search parameters were applied: carbamidomethylation of cysteines was set as a fixed modification, oxidation of methionine and protein N-terminal acetylation were set as variable modifications. The mass tolerances in MS and MS/MS were set to 5 ppm and 20 ppm respectively. Maximum peptide charge was set to 7 and 5 amino acids were required as minimum peptide length. At least 2 peptides (including 1 unique peptides) were asked to report a protein identification. A false discovery rate of 1% was set up for both protein and peptide levels. iBAQ value was calculated. The match between runs features was allowed for biological replicate only.

Data analysis for quantitative proteomics. Quantitative analysis was based on pairwise comparison of protein intensities. Values were log-transformed (log2). Reverse hits and potential contaminant were removed from the analysis. Proteins with at least 2 peptides were kept for further statistics after removing shared proteins from the uninfected GFP alone control. Intensity values were normalized by median centering within conditions (normalized function of the R package DAPAR [77]). Remaining proteins without any iBAQ value in one of both conditions have been considered as proteins quantitatively present in a condition and absent in the other. They have therefore been set aside and considered as differentially abundant proteins. Next, missing values were imputed using the impute. MLE function of the R package imp4p (https://rdrr.io/cran/imp4p/man/imp4p-package.html). Statistical testing was conducted using a limma t-test thanks to the R package limma [78]. An adaptive Benjamini-Hochberg procedure was applied on the resulting p-values thanks to the function adjust.p of R package cp4p[79] using the robust method described in ([80]) to estimate the proportion of true null

hypotheses among the set of statistical tests. The proteins associated to an adjusted p-value inferior to a FDR level of 1% have been considered as significantly differentially abundant proteins.

Statistical analysis. All experiments, unless otherwise noted, were biologically repeated 3–5 times and the statistical test is reported in the figure legend. Data normality was tested by Shapiro-Wilk test, and appropriate parametric or non-parametric tests performed depending on result. P values calculated using GraphPad Prism software and the exact values are in source data. Microscopy data obtained from analysis of 3 – 5 image fields per biological replicate after being automatically acquired by the microscope software to ensure unbiased sampling with the total number of analyzed cells or nuclei noted in the figure legend.

Data Availability:

All data in the present study is available upon request from the corresponding authors.

Code Availability:

No custom code or software was used in the manuscript.

Acknowledgements:

We would like to thank Emmanuelle Varon and Thomas Kohler for their generous gifts of *S. pneumonie* strains. We are appreciative of Pierre-Henri Commere and the Institut Pasteur, Flow Cytometry Platform (Paris, France) for sorting of the COMMD2 stable cell line. Biostatistics and R scripts generated through discussion with Sebastian Baumgarten (Plasmodium RNA Biology; Institut Pasteur) were greatly appreciated. Finally, we like to thank Daniel Hamaoui for his help processing blots during COVID-19 related work personnel restrictions. Michael G. Connor is supported by a Springboard to Independence grant (AirwayStasis) from the French Government's Investissement d'Avenir program, the Laboratoire d'Excellence ''Integrative Biology of Emerging Infectious Diseases" (ANR-10-LABX-62-IBEID). Work in the laboratory Chromatin and infection unit (headed by Melanie A. Hamon) is supported by the Institut Pasteur, the Fondation pour la Recherche Médicale (FRM-EQU202003010152), the Fondation iXCore-iXLife and the Pasteur-Weizmann research fund. Caroline M. Weight was supported by the Medical Research Council (MR/T016329/1). We would like to thank Robert S. Heyderman (UCL) for in depth discussion on the manuscript and he is supported by the MRC (MR/T016329/1). RSH is a National Institute for Health Research (NIHR) Senior Investigator. The views expressed in this article are those of the authors and not necessarily those of the NIHR, or the Department of Health and Social Care. Jost Enninga and Lisa Sanchez, members of Dynamics of host-pathogen interactions unit (Institut Pasteur), are supported by the European Commission (ERC-CoG-Endosubvert), the ANR-HBPsensing, and are members of the IBEID and Milieu Interieur LabExes.

Author contributions:

Conceived and designed all experiments: MGC and MAH. Performed and analyzed data for all experiments: MGC with specific contributions from LS (confocal microscopy imaging repeats); FC, MGE, & TC (p65 mass spectrometry data, repeats for GFP & endogenous immunoprecipitations validations, analysis…) CMW (Detroit562 immunoblot). MGC and MAH edited and reviewed the manuscript. MAH supervised the research and secured funding. All authors approved the final manuscript.

Conflict of interest statement:

The authors declare no conflict of interest.

Figure 1: TIGR4 antagonizes p65 activation. Immunoblot of A549 human airway epithelial cells 2 hrs post-challenge with either IL-1β (10 ng/ml), TIGR4 (MOI 20) or 6B ST90 (MOI 20) (+/- IL-1β; 10 ng/ml). Whole cell lysates probed for p65, phosphorylated p65 at Serine 276, phosphorylated p65 at Serine 536 or Actin. A) Representative image of immunoblot. Actin normalized B) total p65, C) phosphorylated p65 at Serine 276 and D) phosphorylated p65 at Serine 536 (n=11 biological replicates). Dot blot with mean (red line). One-way ANOVA with repeated measures with mixed-effects analysis comparing all means with Tukey's multiple comparison post-hoc test. **P ≤ 0.01, ***P ≤ 0.001, ****P ≤ 0.0001. Full blots provided in Supplementary Information 1.

Figure 2: TIGR4 represses p65 dependent transcription. Immunofluorescence confocal microscopy of paraformaldehyde fixed A549 cells 2 h post-challenge with either IL-1β (10 ng/ml) or TIGR4 (+/- IL-1β 10 ng/ml; MOI 20) stained for p65 (cyan) and nucleus (DAPI; gray). Scale bar = 100μm. B) Quantification of nuclear p65 normalized to the nuclei (n = 3 biological replicates with total nuclei counts for Uninfected n= 636, IL-1β n= 801, TIGR4 n=633, TIGR4 + IL-1β n=516). Tukey box and whisker plot with defined box boundaries being the upper and lower interquartile range (IQR), 'whiskers' (fences) being ± 1.5 times IQR and the median depicted by the middle solid line. Dots represent outliers. Two-way ANOVA comparing all means with Tukey's multiple comparison post-hoc test. ****P ≤ 0.0001. C) RT-qPCR IL-6, IL-8, PTGS2 & CSF2 transcript profiles of A549 cells over a 2 hr time course challenged with either IL-1β or TIGR4 (+/- IL-1β 10 ng/ml; MOI 20). Graphed as the relative expression of each indicated transcript to matched uninfected/unstimulated control per time point (n = 3 biological replicates; 2 technicals per replicate). Displayed as a dot plot with each data point and a bar representing the mean. Chromatin was obtained from A549 cells either untreated (light gray), IL-1β treated (10 ng/ml; dark gray) or 2 hrs post-challenge with TIGR4 (light blue; MOI 20). D) Schematic representation of PTGS2 promoter with ChIP-qPCR primer locations (P1 & P2) and NF-κB sites [63]. E & F) ChIP-qPCR represented as % recovery against input of p65 at indicated NF-κB sites. Tukey box and whisker plot with defined box boundaries being the upper and lower interquartile range (IQR), 'whiskers' (fences) being ± 1.5 times IQR and the median depicted by the middle solid line (n=3 biological replicates with 2 technicals per replicate). One-way ANOVA comparing all means with Tukey's multiple comparison post-hoc test. *P ≤ 0.05, **P ≤ 0.01, ***P ≤ 0.001.

Figure 3: TIGR4 induces a divergent p65 interactome leading to NF-kB p65 turnover by aggrephagy. Mass-spectrometry interactome (n=4 biological replicates per condition) of immunoprecipitated GFP-p65 from a stable A549 GFP-p65 cell line ($1x10^7$ cells total) 2 hrs post challenge with either 6B ST90 (MOI 20) or TIGR4 (MOI 20). A) Volcano plot of identified interacting partners with known NF-kB p65 partners in blue and general significant targets in yellow. Lines represent FDR and fold-change cutoffs with targets of interested denoted. B) Representative immunoblot of A549 whole cell lysates 2 hrs post-challenge with either IL-1β (10 ng/ml), TIGR4 (MOI 20) or 6B ST90 (MOI 20) (+/- IL-1β; 10 ng/ml) probed for RelB, HDAC6, or Actin. C & D) Quantification of RelB or HDAC6 levels normalized to Actin (n=4 biological replicates). Displayed as a dot blot with mean (red line). One-way ANOVA with repeated measures with mixed-effects analysis comparing all means. *P ≤ 0.05, **P ≤ 0.01, ***P ≤ 0.001. Whole cell lysates from A549 cells 2 hrs post-challenge with either IL-1β (10 ng/ml) or TIGR4 (MOI 20; +/- IL-1β; 10 ng/ml) from E) Bafilomycin A1 (400nM) or G) SAR405 (500nM) pretreated cells (both 3 hrs) and immunoblots probed for p65 or actin (n=3 biological replicates). Quantified levels of total p65 normalized to actin from F) Bafilomycin A1 (400nM) or H) SAR405 (500nM). Dot blot with mean (red line). One-way ANOVA with repeated measures with mixed-effects analysis comparing all means. ns = not significant. Full blots provided in Supplementary Information 2

Figure 4: TIGR4 drives NF-kB p65 interaction with COMMD2 and p62 (SQSTM1) and nuclear translocation. Immunoprecipitates using GFP-Trap agarose beads were collected from a stable A549 GFP-COMMD2 cell line 2 hrs post-challenge with either IL-1β (10 ng/ml) or TIGR4 (MOI 20; +/- IL-1β; 10 ng/ml). A) A single representative immunoblot from 3 biological replicates of GFP-COMMD2 immunoprecipitation lysates (input & IP) probed for p65 or GFP.. B) Representative immunoblot from 3 biological replicates of GFP-COMMD2 immunoprecipitation lysates (input & IP) probed for p62 or GFP.. Full blots provided in Supplementary Information 3. C) Immunofluorescence confocal microscopy of stable A549 GFP-COMMD2 cells 2 h post-challenge with either IL-1β (10 ng/ml) or TIGR4 (+/- IL-1β 10 ng/ml; MOI 20) stained for p62 (magenta) against GFP-COMMD2 (gray). Scale bar = 100 µm. Red inset images of single cell highlighting (white arrow) perinuclear punta. Inset scale bar 10 µm. Quantification of total cellular p62 D) normalized to cell area (GFP-COMMD2 signal) and nuclear p62 E) normalized to the area of the nucleus (DAPI signal; n = 3 biological replicates with total cell counts for Uninfected n= 548, IL-1β n= 670, TIGR4 n=356, TIGR4 + IL-1β n=271). Quantification of total cellular COMMD2 F) normalized to cell area (GFP-COMMD2 signal) and nuclear COMMD2 G) normalized to the area of the nucleus (DAP I signal; n = 3 biological replicates with total cell counts for Uninfected n= 864, IL-1β n= 1068, TIGR4 n=596, TIGR4 + IL-1β n=534). Tukey box and whisker plot with defined box boundaries being the upper and lower interquartile range (IQR), 'whiskers' (fences) being ± 1.5 times IQR and the median depicted by the middle solid line. Dots represent outliers. Two-way ANOVA comparing all means with Tukey's multiple comparison post-hoc test. **P ≤ 0.01, ***P ≤ 0.001, ****P ≤ 0.0001. H) Cell fractions from a stable A549 GFP-COMMD2 cell line 2 hrs post-challenge with either IL-1β (10 ng/ml) or TIGR4 (MOI 20; +/- IL-1β; 10 ng/ml). Representative immunoblot probed for GFP (COMMD2) enrichment across cellular compartments. GapDH or histone H4 (H4) used to determine fraction purity. Full blots provided in Supplementary Information 3. I) Percent nuclear COMMD2 levels normalized to input (n=3 biological replicates). Graphed as mean ± STD with dots representing individual biological replicates. One-way ANOVA with repeated measures with mixed-effects analysis comparing all means with Tukey's multiple comparison post-hoc test. ****P ≤ 0.0001.

Figure 5: TIGR4 challenge triggers COMMD2 nuclear localization in a Ply dependent manner. A) Immunofluorescence deconvolution epifluorescence microscopy of paraformaldehyde fixed stable A549 GFP-COMMD2 cells 2 h post-challenge with either IL-1β (10 ng/ml), TIGR4 wildtype (MOI 20), TIGR4 *Δply* (MOI 20), or TIGR4 *ΔspxB* (MOI 20) with GFP-COMMD2 (gray). Scale bar = 10µm. B) Quantification of nuclear GFP-COMMD2 normalized to the segmented nuclei using DAPI signal (omitted in representative images for phenotype clarity; n = 3 biological replicates with total nuclei counts for Uninfected n= 6292, IL-1β n= 6579, TIGR4 n=5061, TIGR4 ΔPly n=7607, TIGR4 ΔSpxB n=6566). Graphed as mean ± STD with dots representing individual biological replicates. One-way ANOVA comparing all means with Tukey's multiple comparison post-hoc test. *P ≤ 0.05, **P ≤ 0.01.

Figure 6: COMMD2-p65-p62 is exported from nucleus through CRM1. Immunofluorescence confocal microscopy of stable A549 GFP-COMMD2 pretreated for 3 hrs with Leptomycin B (10 nM) prior to 2 hr challenge with either IL-1β (10 ng/ml) or TIGR4 (MOI 20). Paraformaldehyde fixed cells stained for A) p62 (magenta), or B) p65 (cyan) against GFP-COMMD2 (gray) and nuclei (DAPI; blue). Scale bar = 100 µm or 10 µm for uninfected and untreated single cell inserts. Nuclear levels of C) GFP-COMMD2 or D) p62 normalized to the segmented nuclei using DAPI signal (n = 3 biological replicates with total nuclei counts for Uninfected (-) n=1664, Uninfected n= 742, IL-1β (-) n=1068, IL-1β n= 920, TIGR4 (-) n=585, TIGR4 n=798). E) Nuclear levels of p65 normalized to the segmented nuclei using DAPI signal (n = 3 biological replicates with total nuclei counts for Uninfected (-) n=489, Uninfected n= 1492, IL-1β (-) n=576 IL-1β n= 1658, TIGR4 (-) n=680, TIGR4 n=1514). Tukey box and whisker plot with defined box boundaries being the upper and lower interquartile range (IQR), 'whiskers' (fences) being ± 1.5 times

IQR and the median depicted by the middle solid line. Dots represent outliers. Two-way ANOVA comparing all means with Tukey's multiple comparison post-hoc test. ***P ≤ 0.001, ****P ≤ 0.0001.

Figure 7: COMMD2-p62 export NF-kB p65 for degradation. Representative immunofluorescence confocal microscopy of stable A549 GFP-COMMD2 pretreated for 3 hrs with Leptomycin B (10nM) prior to 2 hr challenge TIGR4 (MOI 20; +/- IL-1β; 10 ng/ml). Paraformaldehyde fixed cells stained for (A) p62 (magenta) against GFP-COMMD2 (gray) and nuclei (DAPI; blue). Scale bar = 10μm B) Nuclear p62 puncta quantification (n = 3 biological replicates with total nuclei counts for Uninfected n=1041, IL-1β n=831, TIGR4 n=1164, TIGR4 + IL-1β n=1269). Graphed as mean ± STD with dots representing individual biological replicates. One-way ANOVA comparing all means with Tukey's multiple comparison post-hoc test. *P ≤ 0.05, **P ≤ 0.01, ****P ≤ 0.0001. C) Quantified immunofluorescence confocal microscopy of A549 GFP-COMMD2 cells pretreated with Bafilomycin A1 (400nM; 3 hrs) prior to 2 hr challenge with either IL-1β (10 ng/ml) or TIGR4 (MOI 20; +/- IL-1β; 10 ng/ml). Paraformaldehyde fixed and stained for C) p65, D) COMMD2 or E) p62. (n = 3 biological replicates with total cell count for Uninfected p62 & COMMD2 n=1648 & p65 n=1496, IL-1β p62 & COMMD2 n=2103 & p65 n=1703, TIGR4 p62 & COMMD2 n=2033 & p65 n=1597, TIGR4 + IL-1β p62 & COMMD2 n=1724 & p65 n=1759). Tukey box and whisker plot with defined box boundaries being the upper and lower interquartile range (IQR), 'whiskers' (fences) being ± 1.5 times IQR and the median depicted by the middle solid line. Dots represent outliers. Two-way ANOVA comparing all means with Tukey's multiple comparison post-hoc test. ns=not significant, ***P ≤ 0.001,****P ≤ 0.0001.

Sup. Figure 1: TIGR4 actively dampens p65 activation over time. A) Representative graph of actin normalized phosphorylated p65 S536 levels over 2 hrs quantified by immunoblot. B) Immunoblot of whole cell lysates obtained from primary human nasal epithelial cells 2 hrs post-challenge with either IL-1β (10 ng/ml), TIGR4 (MOI 20) or 6B ST90 (MOI 20) (+/- IL-1β; 10 ng/ml). PVDF membrane probed for phosphorylated p65 Serine 536 or Actin (n=2 biological replicates). C) Immunoblot of whole cell Detroit 562 cell lysates 2 hrs post-challenge with either TIGR4 (MOI 10) or 6B ST90 (MOI 10). Nitrocellulose membrane probed for phosphorylated p65 Serine 536 or GapDH (n=2 biological replicates).

Sup. Figure 2: Proteasomal degradation is not involved in TIGR4 mediated p65 turnover. A) Quantification and representative immunoblot image of MG132 (10μM; 3 hr pretreatment) treated A549 whole cell lysates 2 hrs post-challenge with either IL-1β (10 ng/ml), TIGR4 (MOI 20) or 6B ST90 (MOI 20) (+/- IL-1β; 10 ng/ml) and probed for total p65 or actin (n=11 biological replicates). Dot blot with mean (red line). One-way ANOVA with repeated measures with mixed-effects analysis comparing all means with Tukey's multiple comparison post-hoc test. ns=not significant, ****P ≤ 0.0001. B) Representative immunoblot of whole cell lysates collected from primary human nasal epithelial cells treated with Bafilomycin A1 (400nM; 3 hrs) prior to 2 hr challenge with either IL-1β (10 ng/ml) or TIGR4 (MOI 20; +/- IL-1β; 10 ng/ml). PVDF membrane probed for levels of p65 and actin. C) Representative immunoblot of endogenous p65 immunoprecipitation (input & IP) from $1x10^7$ A549 cells post 2 hr challenge using protein G sepharose beads. Collected lysates probed for p65, RelB or NFkB1 (p105/p50).

Sup. Figure 3: TIGR4 specifically drives COMMD2 translocation and induces aggrephagy. A) Cell fractions from a stable A549 GFP-COMMD2 cell line 2 hrs post-challenge with either IL-1β (10 ng/ml), TIGR4 (MOI 20) or 6B ST90 (MOI 20). Representative immunoblot of cell fractions and coomassie stained PVDF membranes. Blots probed for GFP (COMMD2) enrichment across cellular compartments. B) Representative immunoblot of A549 whole cell lysates 2 hrs post-challenge with either IL-1β (10

772 ng/ml) or TIGR4 (MOI 20) obtained from untreated or pretreated (3 hrs) with Bafilomycin A1 (400nM).
773 PVDF membrane probed for p62 or actin. Table is the quantification of actin normalized p62 levels
774 across conditions.

References

1 Ghosh, S. & Hayden, M. S. New regulators of NF-kappaB in inflammation. *Nature reviews. Immunology* **8**, 837-848, doi:10.1038/nri2423 (2008).

2 Bhatt, D. & Ghosh, S. Regulation of the NF-kappaB-Mediated Transcription of Inflammatory Genes. *Frontiers in immunology* **5**, 71, doi:10.3389/fimmu.2014.00071 (2014).

3 Rahman, M. M. & McFadden, G. Modulation of NF-κB signalling by microbial pathogens. *Nature Reviews Microbiology* **9**, 291-306, doi:10.1038/nrmicro2539 (2011).

4 Brücher, B., Lang, F. & Jamall, I. NF-kB signaling and crosstalk during carcinogenesis. *4open* **2**, 1-35, doi:10.1051/fopen/2019010 (2019).

5 Hoffmann, A., Natoli, G. & Ghosh, G. Transcriptional regulation via the NF-κB signaling module. *Oncogene* **25**, 6706-6716, doi:10.1038/sj.onc.1209933 (2006).

6 Basak, S. & Hoffmann, A. Crosstalk via the NF-kappaB signaling system. *Cytokine & growth factor reviews* **19**, 187-197, doi:10.1016/j.cytogfr.2008.04.005 (2008).

7 Shih, V. F.-S., Tsui, R., Caldwell, A. & Hoffmann, A. A single NFκB system for both canonical and non-canonical signaling. *Cell research* **21**, 86-102, doi:10.1038/cr.2010.161 (2011).

8 Huxford, T. & Ghosh, G. A structural guide to proteins of the NF-kappaB signaling module. *Cold Spring Harbor perspectives in biology* **1**, a000075, doi:10.1101/cshperspect.a000075 (2009).

9 Wong, D. *et al.* Extensive characterization of NF-κB binding uncovers non-canonical motifs and advances the interpretation of genetic functional traits. *Genome biology* **12**, R70-R70, doi:10.1186/gb-2011-12-7-r70 (2011).

10 Christian, F., Smith, E. L. & Carmody, R. J. The Regulation of NF-κB Subunits by Phosphorylation. *Cells* **5**, 12, doi:10.3390/cells5010012 (2016).

11 Oeckinghaus, A. & Ghosh, S. The NF-κB Family of Transcription Factors and Its Regulation. *Cold Spring Harbor perspectives in biology* **1**, a000034, doi:10.1101/cshperspect.a000034 (2009).

12 Bartuzi, P., Hofker, M. H. & van de Sluis, B. Tuning NF-κB activity: A touch of COMMD proteins. *Biochimica et Biophysica Acta (BBA) - Molecular Basis of Disease* **1832**, 2315-2321, doi:https://doi.org/10.1016/j.bbadis.2013.09.014 (2013).

13 Newton, K. & Dixit, V. M. Signaling in innate immunity and inflammation. *Cold Spring Harbor perspectives in biology* **4**, doi:10.1101/cshperspect.a006049 (2012).

14 Burstein, E. *et al.* COMMD proteins, a novel family of structural and functional homologs of MURR1. *The Journal of biological chemistry* **280**, 22222-22232, doi:10.1074/jbc.M501928200 (2005).

15 de Bie, P. *et al.* Characterization of COMMD protein-protein interactions in NF-kappaB signalling. *The Biochemical journal* **398**, 63-71, doi:10.1042/BJ20051664 (2006).

16 Maine, G. N., Mao, X., Komarck, C. M. & Burstein, E. COMMD1 promotes the ubiquitination of NF-kappaB subunits through a cullin-containing ubiquitin ligase. *Embo J* **26**, 436-447, doi:10.1038/sj.emboj.7601489 (2007).

17 Maine, G. N. & Burstein, E. COMMD proteins and the control of the NF kappa B pathway. *Cell Cycle* **6**, 672-676, doi:10.4161/cc.6.6.3989 (2007).

18 Maine, G. N. & Burstein, E. COMMD proteins: COMMing to the scene. *Cellular and molecular life sciences : CMLS* **64**, 1997-2005, doi:10.1007/s00018-007-7078-y (2007).

19 Riera-Romo, M. COMMD1: A Multifunctional Regulatory Protein. *Journal of cellular biochemistry* **119**, 34-51, doi:10.1002/jcb.26151 (2018).

20 Geng, H., Wittwer, T., Dittrich-Breiholz, O., Kracht, M. & Schmitz, M. L. Phosphorylation of NF-kappaB p65 at Ser468 controls its COMMD1-dependent ubiquitination and target gene-specific proteasomal elimination. *EMBO Rep* **10**, 381-386, doi:10.1038/embor.2009.10 (2009).

21 Thoms, H. C. *et al.* Nucleolar Targeting of RelA(p65) Is Regulated by COMMD1-Dependent Ubiquitination. *Cancer research* **70**, 139-149, doi:10.1158/0008-5472.Can-09-1397 (2010).

22 Mao, X. *et al.* COMMD1 (copper metabolism MURR1 domain-containing protein 1) regulates Cullin RING ligases by preventing CAND1 (Cullin-associated Nedd8-dissociated protein 1)

binding. *The Journal of biological chemistry* **286**, 32355-32365, doi:10.1074/jbc.M111.278408 (2011).

23 Johannessen, M., Askarian, F., Sangvik, M. & Sollid, J. E. Bacterial interference with canonical NFκB signalling. *Microbiology (Reading, England)* **159**, 2001-2013, doi:10.1099/mic.0.069369-0 (2013).

24 Connor, M. G. *et al.* The histone demethylase KDM6B fine-tunes the host response to Streptococcus pneumoniae. *Nature Microbiology*, doi:10.1038/s41564-020-00805-8 (2020).

25 Quinton, L. J. *et al.* Functions and regulation of NF-kappaB RelA during pneumococcal pneumonia. *Journal of immunology (Baltimore, Md. : 1950)* **178**, 1896-1903, doi:10.4049/jimmunol.178.3.1896 (2007).

26 Ferreira, D. M. *et al.* Controlled human infection and rechallenge with Streptococcus pneumoniae reveals the protective efficacy of carriage in healthy adults. *American journal of respiratory and critical care medicine* **187**, 855-864, doi:10.1164/rccm.201212-2277OC (2013).

27 Henriques-Normark, B. & Tuomanen, E. I. The Pneumococcus: Epidemiology, Microbiology, and Pathogenesis. *Cold Spring Harbor perspectives in medicine* **3**, a010215, doi:10.1101/cshperspect.a010215 (2013).

28 Jochems, S. P., Weiser, J. N., Malley, R. & Ferreira, D. M. The immunological mechanisms that control pneumococcal carriage. *PLoS pathogens* **13**, e1006665-e1006665, doi:10.1371/journal.ppat.1006665 (2017).

29 Robson, R. L., Reed, N. A. & Horvat, R. T. Differential activation of inflammatory pathways in A549 type II pneumocytes by Streptococcus pneumoniae strains with different adherence properties. *BMC infectious diseases* **6**, 71, doi:10.1186/1471-2334-6-71 (2006).

30 Weight, C. M. *et al.* Microinvasion by Streptococcus pneumoniae induces epithelial innate immunity during colonisation at the human mucosal surface. *Nature communications* **10**, 3060, doi:10.1038/s41467-019-11005-2 (2019).

31 Dong, W. *et al.* Streptococcus pneumoniae Infection Promotes Histone H3 Dephosphorylation by Modulating Host PP1 Phosphatase. *Cell reports* **30**, 4016-4026.e4014, doi:https://doi.org/10.1016/j.celrep.2020.02.116 (2020).

32 Kim, S. *et al.* Stress-induced NEDDylation promotes cytosolic protein aggregation through HDAC6 in a p62-dependent manner. *iScience* **24**, 102146, doi:https://doi.org/10.1016/j.isci.2021.102146 (2021).

33 Lamark, T. & Johansen, T. Aggrephagy: Selective Disposal of Protein Aggregates by Macroautophagy. *International Journal of Cell Biology* **2012**, 736905, doi:10.1155/2012/736905 (2012).

34 Svenning, S. & Johansen, T. Selective autophagy. *Essays in biochemistry* **55**, 79-92, doi:10.1042/bse0550079 (2013).

35 Lee, D. H. & Goldberg, A. L. Proteasome inhibitors: valuable new tools for cell biologists. *Trends in cell biology* **8**, 397-403, doi:10.1016/s0962-8924(98)01346-4 (1998).

36 Mauvezin, C. & Neufeld, T. P. Bafilomycin A1 disrupts autophagic flux by inhibiting both V-ATPase-dependent acidification and Ca-P60A/SERCA-dependent autophagosome-lysosome fusion. *Autophagy* **11**, 1437-1438, doi:10.1080/15548627.2015.1066957 (2015).

37 Dröse, S. & Altendorf, K. Bafilomycins and concanamycins as inhibitors of V-ATPases and P-ATPases. *J Exp Biol* **200**, 1-8, doi:10.1242/jeb.200.1.1 (1997).

38 Pasquier, B. Autophagy inhibitors. *Cellular and molecular life sciences : CMLS* **73**, 985-1001, doi:10.1007/s00018-015-2104-y (2016).

39 Pasquier, B. SAR405, a PIK3C3/VPS34 inhibitor that prevents autophagy and synergizes with MTOR inhibition in tumor cells. *Autophagy* **11**, doi:10.1080/15548627.2015.1033601 (2015).

40 Vonk, W. I. M. *et al.* The Copper Metabolism MURR1 Domain Protein 1 (COMMD1) Modulates the Aggregation of Misfolded Protein Species in a Client-Specific Manner. *PloS one* **9**, e92408, doi:10.1371/journal.pone.0092408 (2014).

41 Johansen, T. & Lamark, T. Selective autophagy mediated by autophagic adapter proteins. *Autophagy* **7**, 279-296 (2011).

42 Johnston, J. A., Ward, C. L. & Kopito, R. R. Aggresomes: a cellular response to misfolded proteins. *The Journal of cell biology* **143**, 1883-1898 (1998).

43 Lobb, I. T. *et al.* A Role for the Autophagic Receptor, SQSTM1/p62, in Trafficking NF-κB/RelA to Nucleolar Aggresomes. *Molecular Cancer Research* **19**, 274, doi:10.1158/1541-7786.MCR-20-0336 (2021).

44 Ryu, H. W., Won, H. R., Lee, D. H. & Kwon, S. H. HDAC6 regulates sensitivity to cell death in response to stress and post-stress recovery. *Cell stress & chaperones* **22**, 253-261, doi:10.1007/s12192-017-0763-3 (2017).

45 Wong, E. *et al.* Molecular determinants of selective clearance of protein inclusions by autophagy. *Nature communications* **3**, 1240, doi:10.1038/ncomms2244 (2012).

46 Weiser, J. N., Ferreira, D. M. & Paton, J. C. Streptococcus pneumoniae: transmission, colonization and invasion. *Nature reviews. Microbiology* **16**, 355-367, doi:10.1038/s41579-018-0001-8 (2018).

47 Kadioglu, A., Weiser, J. N., Paton, J. C. & Andrew, P. W. The role of Streptococcus pneumoniae virulence factors in host respiratory colonization and disease. *Nature reviews. Microbiology* **6**, 288-301, doi:10.1038/nrmicro1871 (2008).

48 Bryant, J. C. *et al.* Pyruvate oxidase of Streptococcus pneumoniae contributes to pneumolysin release. *BMC microbiology* **16**, 271, doi:10.1186/s12866-016-0881-6 (2016).

49 Tan, S. & Wong, E. in *Methods in Enzymology* Vol. 588 (eds Lorenzo Galluzzi, José Manuel Bravo-San Pedro, & Guido Kroemer) 245-281 (Academic Press, 2017).

50 Kudo, N. *et al.* Leptomycin B inactivates CRM1/exportin 1 by covalent modification at a cysteine residue in the central conserved region. *Proceedings of the National Academy of Sciences of the United States of America* **96**, 9112-9117, doi:10.1073/pnas.96.16.9112 (1999).

51 Das, T., Chen, Z., Hendriks, R. W. & Kool, M. A20/Tumor Necrosis Factor α-Induced Protein 3 in Immune Cells Controls Development of Autoinflammation and Autoimmunity: Lessons from Mouse Models. *Frontiers in immunology* **9**, doi:10.3389/fimmu.2018.00104 (2018).

52 Moreno, R., Sobotzik, J.-M., Schultz, C. & Schmitz, M. L. Specification of the NF-κB transcriptional response by p65 phosphorylation and TNF-induced nuclear translocation of IKKε. *Nucleic acids research* **38**, 6029-6044, doi:10.1093/nar/gkq439 (2010).

53 Collins, P. E., Mitxitorena, I. & Carmody, R. J. The Ubiquitination of NF-κB Subunits in the Control of Transcription. *Cells* **5**, 23, doi:10.3390/cells5020023 (2016).

54 Lanucara, F. *et al.* Dynamic phosphorylation of RelA on Ser42 and Ser45 in response to TNFalpha stimulation regulates DNA binding and transcription. *Open Biol* **6**, doi:10.1098/rsob.160055 (2016).

55 Quinton, L. J. & Mizgerd, J. P. Dynamics of lung defense in pneumonia: resistance, resilience, and remodeling. *Annual review of physiology* **77**, 407-430, doi:10.1146/annurev-physiol-021014-071937 (2015).

56 Pechous, R. D. With Friends Like These: The Complex Role of Neutrophils in the Progression of Severe Pneumonia. *Frontiers in cellular and infection microbiology* **7**, 160-160, doi:10.3389/fcimb.2017.00160 (2017).

57 Liu, J. *et al.* Advanced Role of Neutrophils in Common Respiratory Diseases. *Journal of immunology research* **2017**, 6710278, doi:10.1155/2017/6710278 (2017).

58 Craig, A., Mai, J., Cai, S. & Jeyaseelan, S. Neutrophil Recruitment to the Lungs during Bacterial Pneumonia. *Infection and immunity* **77**, 568-575, doi:10.1128/IAI.00832-08 (2009).

59 Pechous, R. D., Sivaraman, V., Stasulli, N. M. & Goldman, W. E. Pneumonic Plague: The Darker Side of Yersinia pestis. *Trends in microbiology*, doi:10.1016/j.tim.2015.11.008 (2015).

60 Yamamoto, K. *et al.* Roles of lung epithelium in neutrophil recruitment during pneumococcal pneumonia. *American journal of respiratory cell and molecular biology* **50**, 253-262, doi:10.1165/rcmb.2013-0114OC (2014).

61 Bou Ghanem, E. N. *et al.* Extracellular Adenosine Protects against Streptococcus pneumoniae Lung Infection by Regulating Pulmonary Neutrophil Recruitment. *PLoS pathogens* **11**, e1005126, doi:10.1371/journal.ppat.1005126 (2015).

62 Livak, K. J. & Schmittgen, T. D. Analysis of relative gene expression data using real-time quantitative PCR and the 2(-Delta Delta C(T)) Method. *Methods (San Diego, Calif.)* **25**, 402-408, doi:10.1006/meth.2001.1262 (2001).

63 Nguyen, L. K., Cavadas, M. A. S., Kholodenko, B. N., Frank, T. D. & Cheong, A. Species differential regulation of COX2 can be described by an NFκB-dependent logic AND gate. *Cellular and molecular life sciences : CMLS* **72**, 2431-2443, doi:10.1007/s00018-015-1850-1 (2015).

64 Huang, F., Spangler, J. R. & Huang, A. Y. In vivo cloning of up to 16 kb plasmids in E. coli is as simple as PCR. *PloS one* **12**, e0183974, doi:10.1371/journal.pone.0183974 (2017).

65 Watson, J. F. & García-Nafría, J. In vivo DNA assembly using common laboratory bacteria: A re-emerging tool to simplify molecular cloning. *The Journal of biological chemistry* **294**, 15271-15281, doi:10.1074/jbc.REV119.009109 (2019).

66 Thuring, R. W., Sanders, J. P. & Borst, P. A freeze-squeeze method for recovering long DNA from agarose gels. *Analytical biochemistry* **66**, 213-220, doi:10.1016/0003-2697(75)90739-3 (1975).

67 Tautz, D. & Renz, M. An optimized freeze-squeeze method for the recovery of DNA fragments from agarose gels. *Analytical biochemistry* **132**, 14-19, doi:10.1016/0003-2697(83)90419-0 (1983).

68 Jin, Z. *et al.* The hyperactive Sleeping Beauty transposase SB100X improves the genetic modification of T cells to express a chimeric antigen receptor. *Gene therapy* **18**, 849-856, doi:10.1038/gt.2011.40 (2011).

69 Kowarz, E., Loscher, D. & Marschalek, R. Optimized Sleeping Beauty transposons rapidly generate stable transgenic cell lines. *Biotechnology journal* **10**, 647-653, doi:10.1002/biot.201400821 (2015).

70 Laemmli, U. K. Cleavage of Structural Proteins during the Assembly of the Head of Bacteriophage T4. *Nature* **227**, 680-685, doi:10.1038/227680a0 (1970).

71 Schindelin, J. *et al.* Fiji: an open-source platform for biological-image analysis. *Nature methods* **9**, 676-682, doi:10.1038/nmeth.2019 (2012).

72 Kamentsky, L. *et al.* Improved structure, function and compatibility for CellProfiler: modular high-throughput image analysis software. *Bioinformatics (Oxford, England)* **27**, 1179-1180, doi:10.1093/bioinformatics/btr095 (2011).

73 McQuin, C. *et al.* CellProfiler 3.0: Next-generation image processing for biology. *PLoS biology* **16**, e2005970, doi:10.1371/journal.pbio.2005970 (2018).

74 Stirling, D. R., Carpenter, A. E. & Cimini, B. A. CellProfiler Analyst 3.0: accessible data exploration and machine learning for image analysis. *Bioinformatics (Oxford, England)* **37**, 3992-3994, doi:10.1093/bioinformatics/btab634 (2021).

75 Kulak, N. A., Pichler, G., Paron, I., Nagaraj, N. & Mann, M. Minimal, encapsulated proteomic-sample processing applied to copy-number estimation in eukaryotic cells. *Nature methods* **11**, 319-324, doi:10.1038/nmeth.2834 (2014).

76 Tyanova, S., Temu, T. & Cox, J. The MaxQuant computational platform for mass spectrometry-based shotgun proteomics. *Nature protocols* **11**, 2301-2319, doi:10.1038/nprot.2016.136 (2016).

77 Wieczorek, S. *et al.* DAPAR & ProStaR: software to perform statistical analyses in quantitative discovery proteomics. *Bioinformatics (Oxford, England)* **33**, 135-136, doi:10.1093/bioinformatics/btw580 (2017).

78 Pounds, S. & Cheng, C. Robust estimation of the false discovery rate. *Bioinformatics (Oxford, England)* **22**, 1979-1987, doi:10.1093/bioinformatics/btl328 (2006).

79 Smyth, G. K. Linear models and empirical bayes methods for assessing differential expression in microarray experiments. *Statistical applications in genetics and molecular biology* **3**, Article3, doi:10.2202/1544-6115.1027 (2004).

80 Giai Gianetto, Q. *et al.* Calibration plot for proteomics: A graphical tool to visually check the assumptions underlying FDR control in quantitative experiments. *Proteomics* **16**, 29-32, doi:10.1002/pmic.201500189 (2016).

FIGURE 1

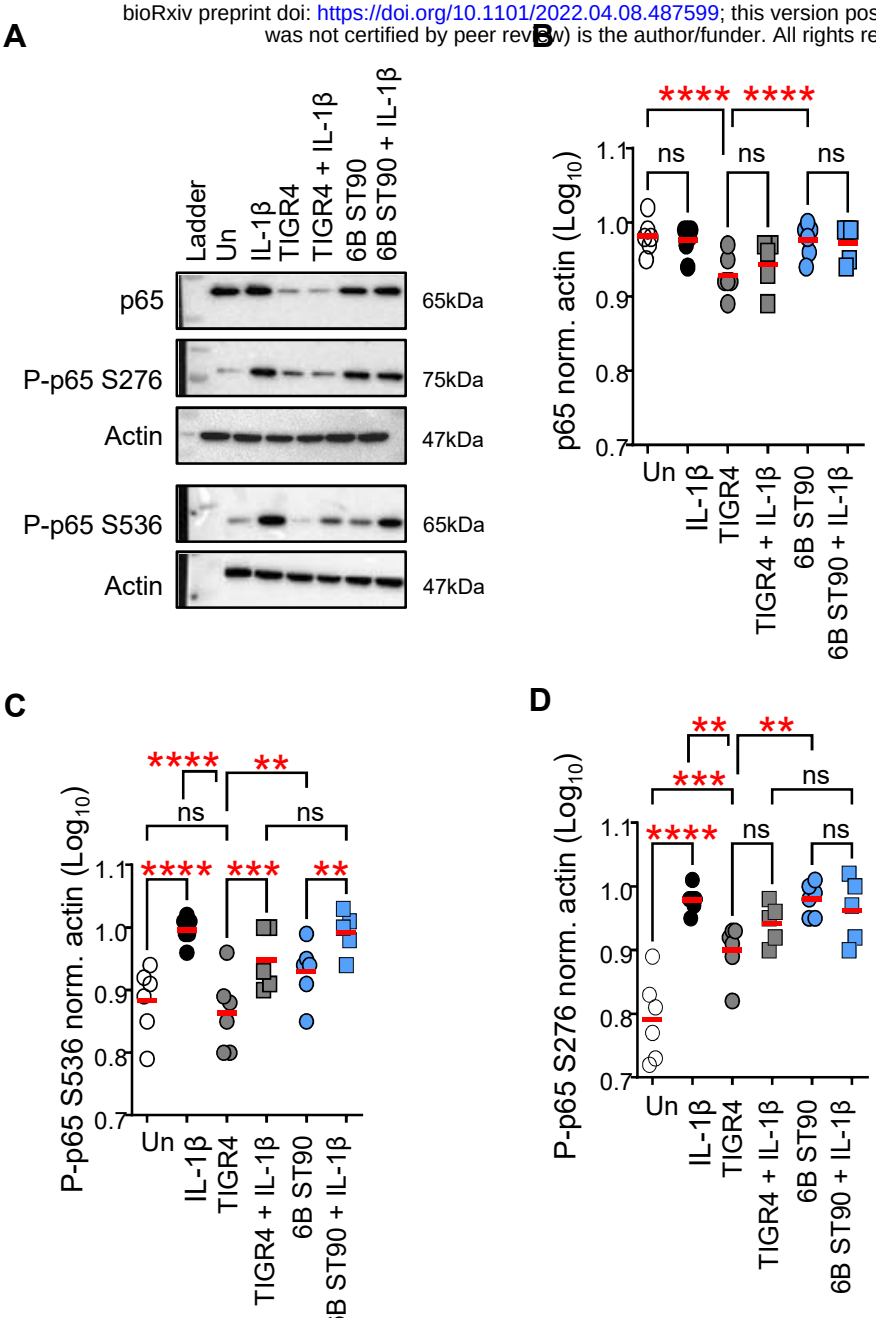

FIGURE 2

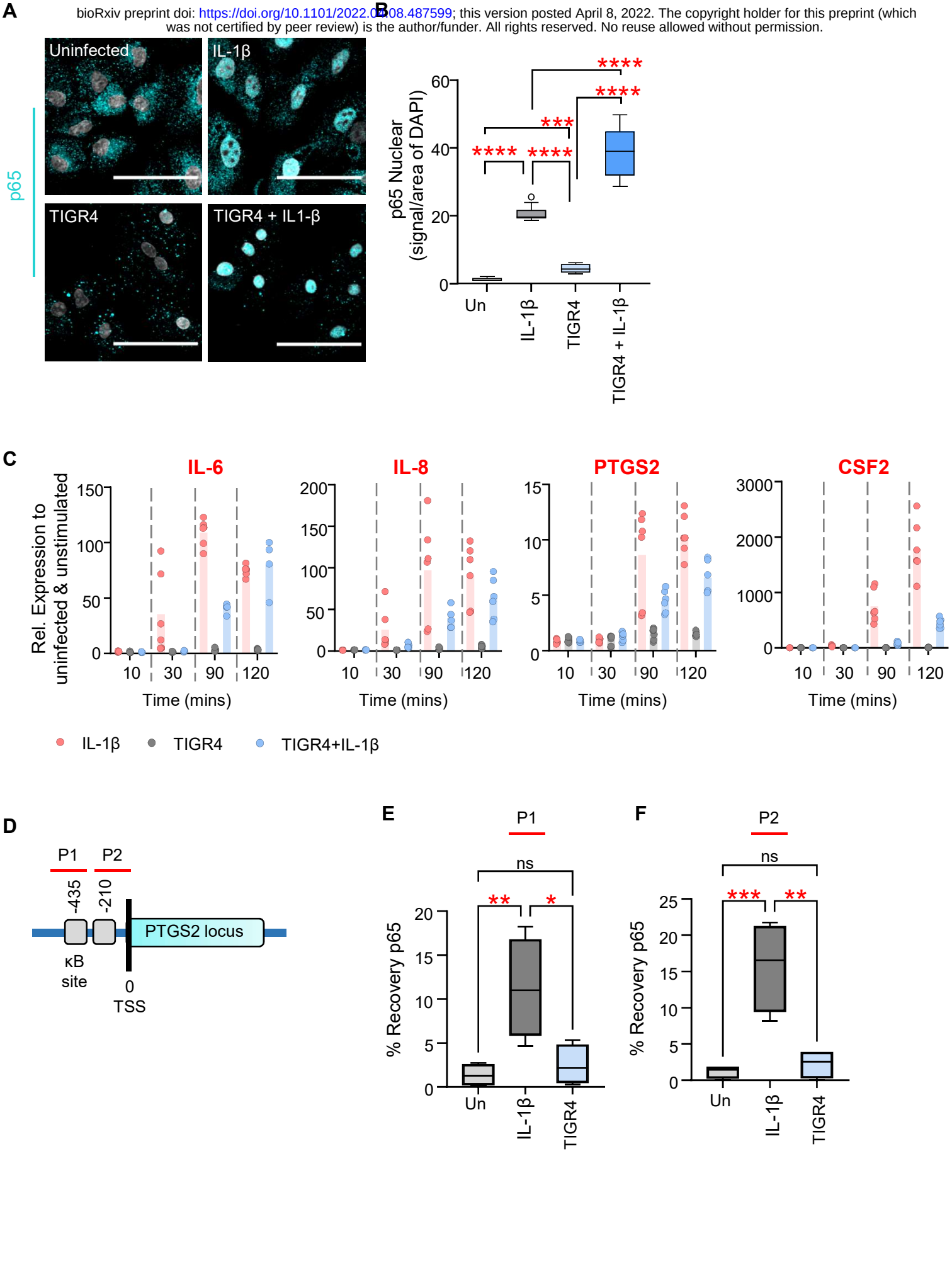

FIGURE 3

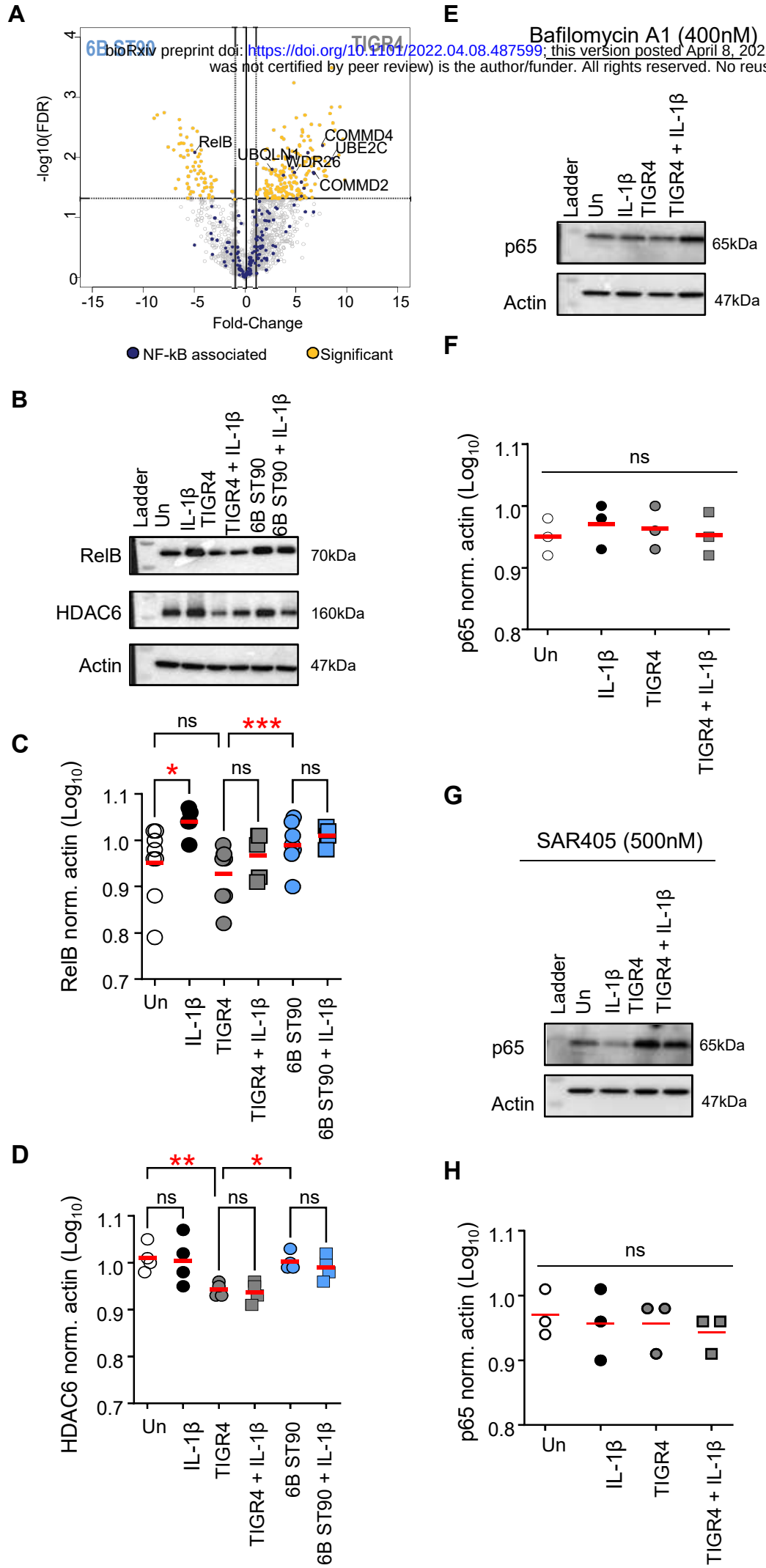

FIGURE 4

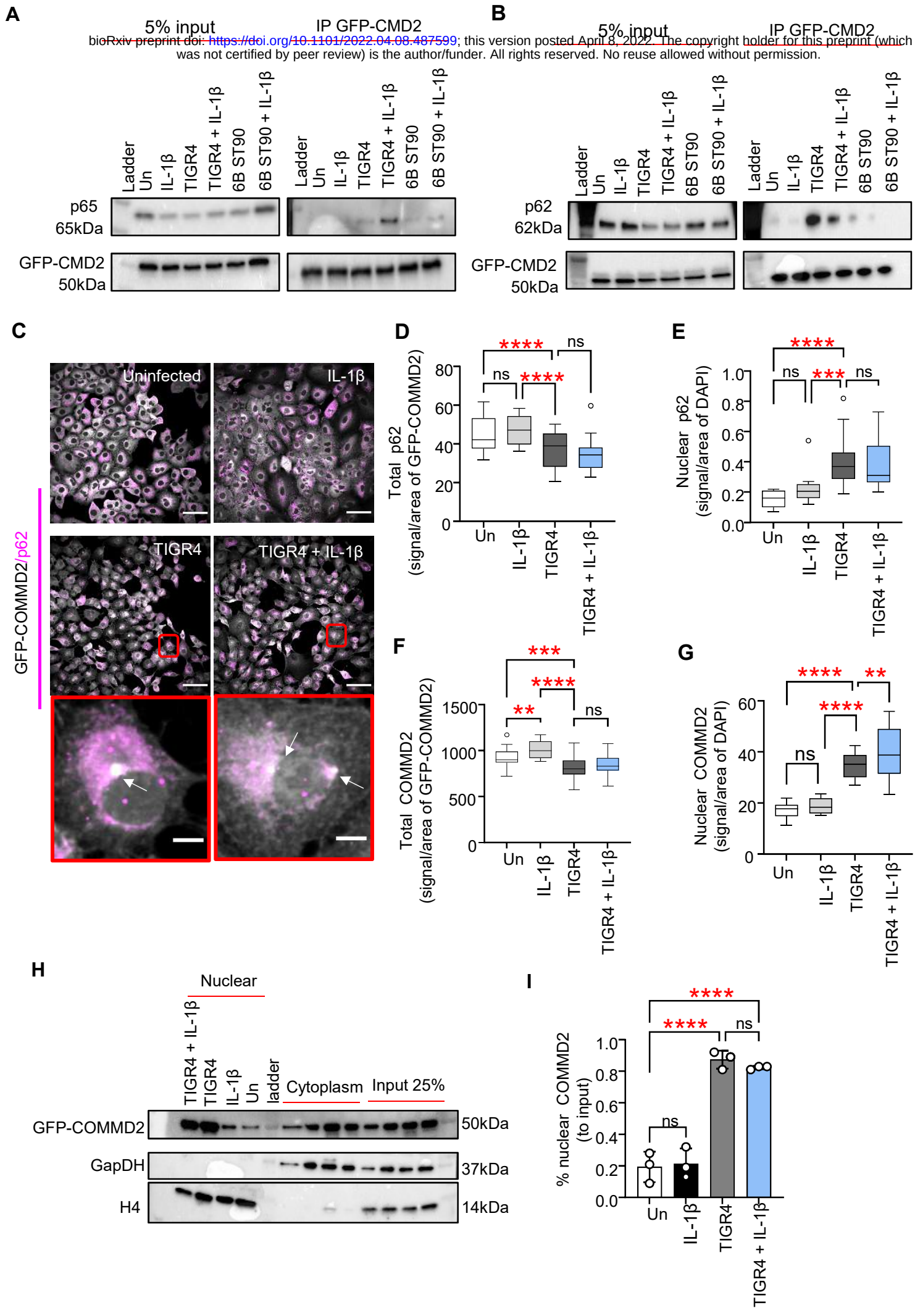

FIGURE 5

A

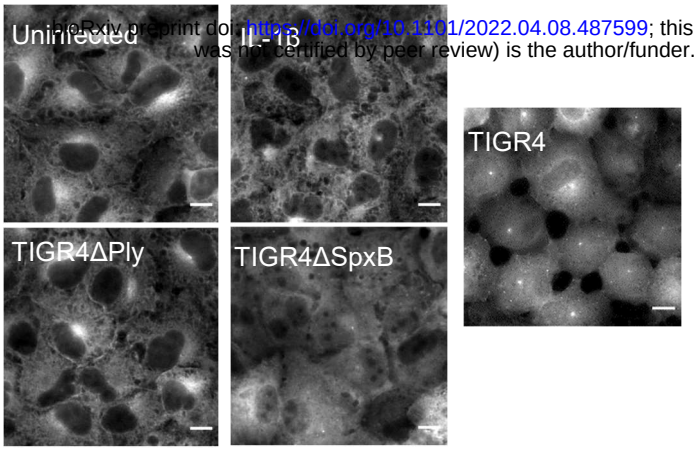

B

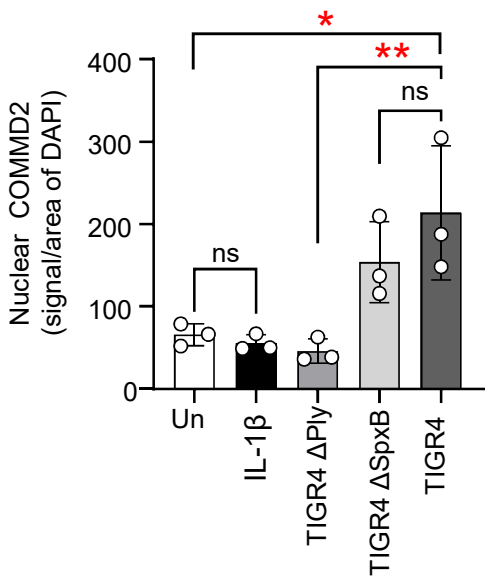

FIGURE 6

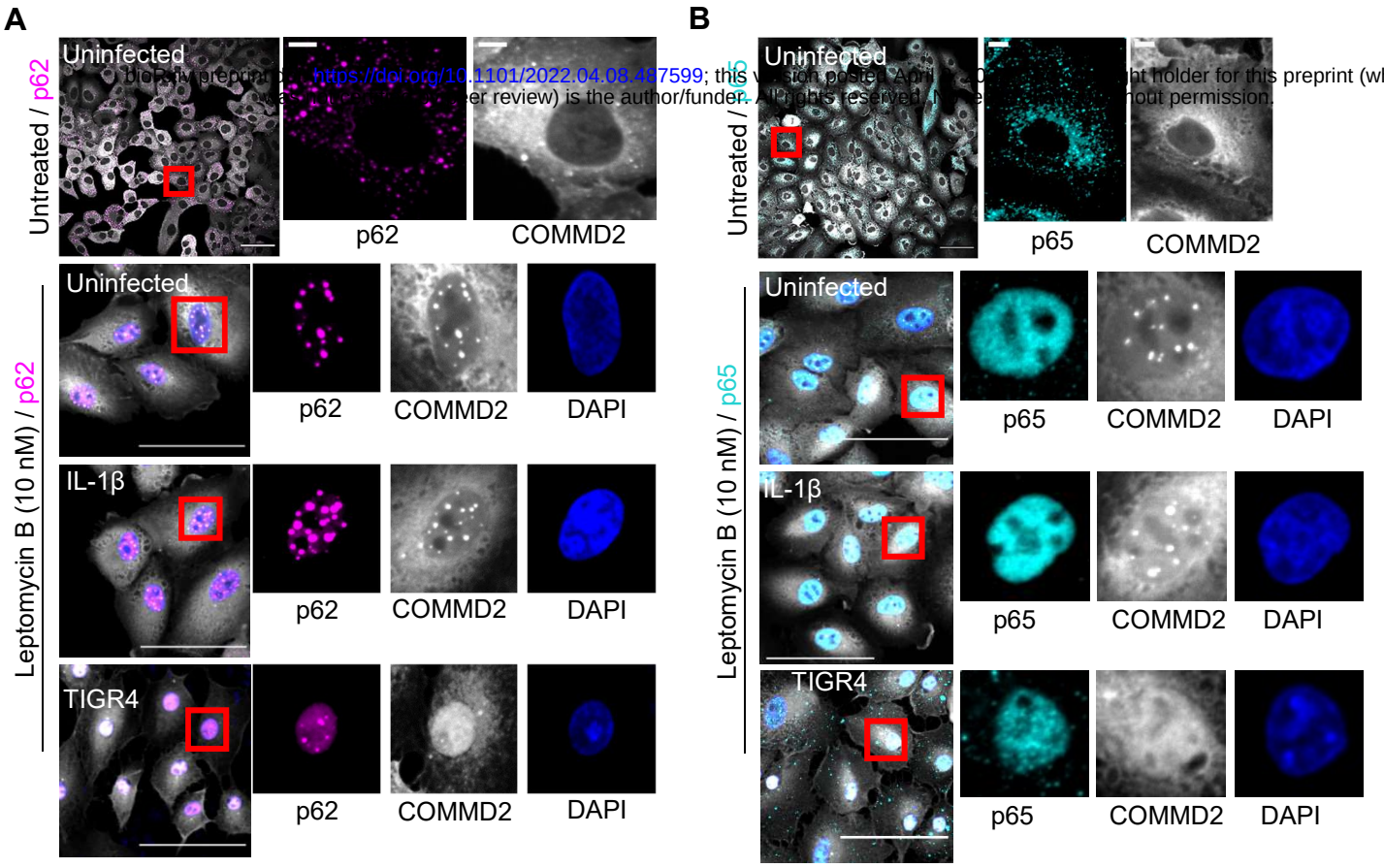

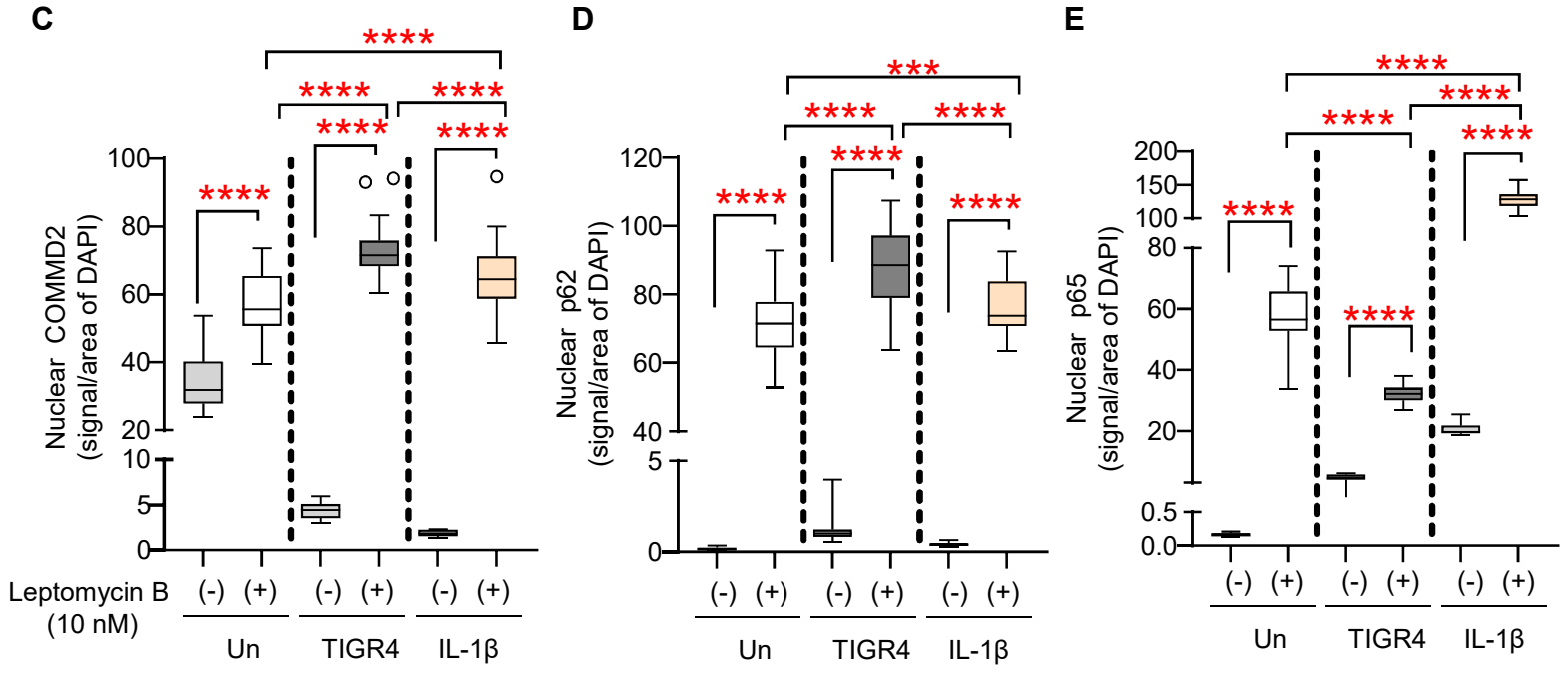

FIGURE 7